Nanotechnology for Environmental Engineering (2024) 9:207–237
https://doi.org/10.1007/s41204-024-00362-z

CRITICAL REVIEWS

Emerging applications of waste fly ash for remediation of environmental contaminants: a high-value and sustainable approach towards utilization of waste materials

Vishal Gadore[1] · Soumya Ranjan Mishra[1] · Mika Sillanpää[2] · Md Ahmaruzzaman[1]

Received: 19 September 2023 / Accepted: 1 February 2024 / Published online: 19 March 2024

Abstract
Fly ash is a greyish-black powdery substance easily available and produced as a side product of burning any organic substance. A huge amount of fly ash is generated worldwide, and today's world faces a severe problem of its disposal. Owing to its various applications, researchers began utilizing fly ash as a catalyst to solve environmental problems. Due to the presence of metal oxides in fly ash, it acts as a good adsorbent. It can be used to support semiconductor photocatalysts in degrading pollutants from wastewater under light irradiation. The current review discusses the preparation methods of fly ash-based materials such as impregnation, wet chemical synthesis, electrospinning, modified meta-organic decomposition, impregnation, sol–gel, layer-by-layer assembly, precipitation/co-precipitation and hydrothermal/solvothermal technique. The application of fly ash and related materials for photocatalytic degradation of organic pollutants and the factors that affect the photodegradation, mechanism, kinetics of photodegradation, and approaches to make photocatalytic degradation more efficient have been reviewed. The techniques used to characterize fly ash nanocomposites, like powdered X-ray diffraction technique, Fourier transform infrared spectroscopy, and scanning electron microscopy, have been discussed to understand the topic better. Furthermore, the applicability of the fly ash and modified fly ash for the sorption of volatile organics, SO*x*, NO*x*, and mercury from flue gases has also been summarized. Moreover, the review also provides a scope for further research in the field of photodegradation and air remediation using fly ash to develop robust and low-cost materials for environmental remediation.

Keywords Adsorbent · Flue gas · Fly ash · Photocatalysts · Nanocomposites

Introduction

Ash is a powdery material generated as a byproduct of the combustion of organic matter. It is mainly utilized by cement manufacturing factories or disposed of in landfills. The Ministry of Power, Government of India, reports that more than 270 million tonnes of fly ash is generated annually. About 1670 million tonnes of fly ash have accumulated over the years due to gross underutilization of this byproduct, according to a report by the Joint Committee in 2021. The disposal of fly ash (FA) has many challenges, like the presence of heavy metals and carcinogenic compounds leading to soil and water pollution. Also, the soil containing FA is unfit for agricultural purposes. Therefore, the problems related to the disposal of FA are a major environmental threat [1]. Hence, scientists are dedicated to developing new methods to utilize FA in an effective and greener way. Much research in recent years has reported using FA and modified FA as an adsorbent to remove heavy elements and dyes from water sources. According to research, the highest adsorption capacity for sulphonated humic acid achieved with pure fly ash was greater than 92 mg/g, which could increase to 321.8 mg/g after modifications [2]. Undoubtedly, FA has emerged as an excellent material for wastewater treatment owing to its greater surface area (170–1000 m^2/g), higher pore size (5–500 nm), and the presence of silicon (15–60%) and aluminium (5–30%) oxides, which act as adsorbents for pollutants [3].

✉ Md Ahmaruzzaman
mda2002@gmail.com

[1] Department of Chemistry, National Institute of Technology Silchar, Assam 788010, India

[2] Department of Chemistry, King Saud University, P.O. Box 2455, Riyadh, Saudi Arabia

Various physical, chemical, and biological techniques have been proposed by researchers for water purification and contaminant removal [4]. Among these techniques, adsorption is an efficient and promising technique for removing hazardous contaminants [5, 6]. Several low-cost adsorbents like metal–organic frameworks (MOFs), activated carbon (AC), carbon nanotubes (CNTs), and fly ash were developed and modified for the efficient removal of toxic metals and hazardous compounds from wastewater and flue gas (FG) [7, 8]. Typical methods of synthesis of CNTs and their selectivity towards particular contaminants limit their practical applications [9]. FA has a good specific surface area (SSA), porosity, particle size, and other natural qualities, making it a low-cost adsorbent without any further modifications [10]. For instance, according to Bhattacharyya et al. [11], FA can be utilized as an adsorbent in a plasma reactor cascade to reduce NOx emissions from biodiesel engines. Hower et al. (2000) showed that FA carbon effectively absorbs Hg from flue gas. Several researchers have discovered that FA is an effective sulphur dioxide (SO_2) and volatile organic compound (VOC) adsorbent after little modification [12]. Other researchers have also successfully documented the one-step electrospun synthesis of fibrous membranes using FA to adsorb volatile organics from the environment [13].

The chemical composition of FA depends on the source, combustion technique, and storage method [14]. Some essential nutrients in FA, like K, B, Cu, Mg, Zn, and Fe, are highly desirable for the healthy growth of some crops [15]. Also, the high concentration of alumina, silica, and iron oxides is essential compounds to enhance the adsorption capacity of FA [16, 17]. The adsorption efficiency of FA can further be improved by alkali activation of SiO_2 and Al_2O_3, resulting in the formation of zeolites.

However, the presence of toxic heavy metals in FA could be a source of secondary pollution. Therefore, scientists found that apart from adsorption, FA could also be used as a base material to anchor semiconductor photocatalysts, further enhancing the removal of pollutants from wastewater. The FA support for semiconductor photocatalysts solved two major problems related to photocatalysts and secondary pollution. Firstly, most of the existing photocatalysts are unstable and easily corroded in an aqueous medium. Therefore, FA enhances the stability of photocatalysts and improves their efficiency by adsorbing pollutants over their surface. Secondly, forming composites of FA suppresses the leachability of heavy metals, which solves the secondary pollution problem.

Titania (TiO_2) is one of the most frequently used photocatalysts, but it has a lower specific surface area (70–100 m^2/g), which reduces the adsorption efficiency [18]. The reaction possesses a low quantum yield due to the higher charge recombination rate [19]. The large bandgap of silica (SiO_2) is similar to TiO_2, which limits its usage only under ultraviolet (UV) light irradiation [20]. Zinc oxide has a non-uniform structure, reducing adsorption capacity and decreasing the photocatalytic reaction's efficiency. Also, ZnO is easily agglomerated under extreme pH (below pH 4 and above pH 9) [21]. Bismuth vanadate ($BiVO_4$) has its own limitations, such as low adsorption efficiency and poor charge-carrying properties [22]. Most photocatalytic reactions involve nano-powdered photocatalysts, which require an extra step for recovery and increase the treatment cost. Therefore, real-world applications of semiconductor materials still experience several disadvantages associated with the recovery and regeneration of the photocatalyst. Many researchers came up with the idea of co-catalyst interactions, immobilization [23], doping [24], and forming a heterojunction with metal oxides to improve the efficiency of a photocatalytic reaction [25, 26]. Recently, the use of FA, activated carbon (AC), clay, etc. for the immobilization of photocatalysts has been widely investigated [27]. Fly ash can float, which serves the purpose of immobility, enhances the exposure of the photocatalyst to light, and helps improve photodegradation performance. After treatment, the photocatalyst can be conveniently rejuvenated from the system [28].

Good research is conducted to find out more about the characteristics and photocatalytic degradation of dyes by fly ash nanocomposites [29, 30]. Coal fly ash (CFA), rice husk ash (RHA), and volcanic ash (VA) are easily available and were generally investigated as supporting materials for photocatalysts to make them more efficient at degrading pollutants owing to their larger surface area, high stability, reusability, and high silica and alumina content [31, 32]. Numerous FA-based photocatalysts with different physicochemical features were prepared and examined for pollutant degradation in water. Due to the high adsorption capacity of the fly ash and the photocatalyst's degradation efficiency, these nanocomposites are particularly effective [33, 34]. Processes like hydrothermal and sol–gel are some of the ways to prepare nanocomposites.

This paper summarizes fly ash's photocatalytic efficiency and adsorptive capacity and related materials to degrade organic contaminants from wastewater and remove toxic gases from the environment. This article aims to deliver a fundamental understanding of FA-based photocatalysts and fly ash as an adsorbent for toxic pollutants from flue gases. This article also summarizes the synthesis of FA-based materials, their properties, characterization techniques, and the photodegradation mechanism of organic contaminants and dyes.

Scope of the review

Various review articles published to date deal with the photocatalytic properties of FA and related materials for the removal of dyes [29, 35]; however, to the best of our

knowledge, no review has been published highlighting the photocatalytic activity of fly ash nanocomposites for the degradation of organic contaminants from water, discussing the mechanism of degradation and application of fly ash in the elimination of toxic gases from the environment in a single article. The review article summarizes the utilization of CFA, RHA, bottom ash, and VA to degrade organic contaminants from wastewater, synthesis techniques, the pros and cons of various synthesis techniques, characterization methods of FA-based materials, factors affecting the photocatalytic process, the mechanism of the degradation of dyes, and the application of fly ash in sorption of toxic gases. This review will help the readers synthesize potent fly ash nanocomposites for environmental remediation. Finally, the challenges and new prospects for designing fly ash-based nanocomposites have been discussed. Over previous years, there has been an exponential increase in the articles published in the field of environmental remediation reporting the use of fly ash as support.

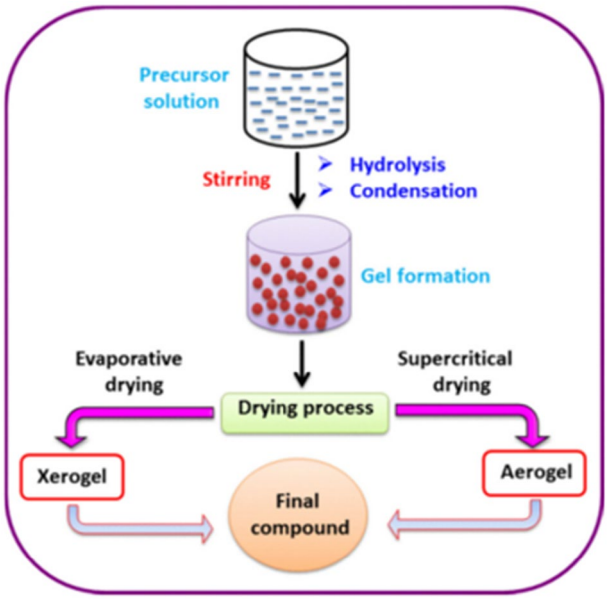

Fig. 1 Sol–gel method to synthesize FA-based nanocomposites [47]

Synthesis of fly ash nanocomposites

Following coal combustion, the bottom 20% of the ash is referred to as bottom ash, and the remaining 80% is transported as fly ash. An electrostatic precipitator is utilized to collect fly ash electrically, and fabric filters are employed as mechanical collecting devices. Fly ash may be collected with 99% efficiency using electrostatic precipitators.

The literature reported the use of RHA, CFA, and VA for the support of photocatalysts. The catalyst type determines the preparation method and the pollutants to remove [36]. It is well known that the adsorption and photodegradation efficiency of nanocomposites are affected by the morphology to a great extent. During the synthesis of nanocomposites, several factors, such as reactant concentration, reaction time, temperature, and use of surfactants and solvents, affect the size and morphology of the nanocomposites [37]. During hydrothermal synthesis, the reaction temperature and the time have a major role in controlling the sample's morphology, while in the sol–gel and precipitation technique, the choice of reactant and stirring speed affects the nanoparticle morphology. The surfactants prevent nanoparticle agglomeration, and their concentration affects the particle size. By adjusting these variables, scientists may optimize the synthesis process and produce nanocomposites with customized morphologies. The following are some standard methods for synthesizing nanocomposites of FA:

Hydrothermal technique

Hydrothermal technique produces nanocomposites with large crystalline sizes (~ 40 to 50 nm), smaller particle sizes (2–50 nm), and a wide range of morphologies (quantum dots, nanosheets, nanorods, nanoflowers, nanospheres) depending upon the reaction conditions [38, 39]. A mixture of metal salt and fly ash is dissolved in water. The solution is transferred to a Teflon-lined autoclave and subjected to high temperatures ranging from 100 to 220 °C. The great purity of the produced sample is due to the nucleation and crystallization reactions that occur inside the tube [40]. Mushtaq et al. [41] fabricated $MnFe_2O_4$/FA nanocomposite using manganese chloride tetrahydrate and ferric nitrate nonahydrate as precursors via a hydrothermal technique at 180 °C for 18 h. The prepared nanocomposite was highly efficient and showed 100% degradation of methylene blue within 30 min.

Sol–gel method

Sol–gel is ideal for producing metal oxide nanoparticles [42]. It is one of the most basic approaches for making nanoparticles [43]. The condensation of metal sols forms a three-dimensional network gel with strong recurring metal–oxygen–metal links. Afterwards, the gel is dried for future use [44]. Water has been used as a solvent; however, this process has since expanded to include organic solvents [45]. The sol–gel approach [46] can be used to dope FA with metals and non-metals. Figure 1 illustrates a sol–gel method to synthesize FA-based nanocomposites [47]. Iron-doped TiO_2 was decorated over FA via a sol–gel method for the removal of methylene blue [48]. Iron and titanium precursors were dissolved in 90 mL ethanol and 10 mL acetylacetone solution. The resultant mixture was

then added to the ethanol solution, followed by ferric nitrate, and the pH was adjusted to 5 by adding HNO_3. After stirring for 1 h at room temperature, 2 g polyethylene glycol was added to the above mixture and stirred for 1 h at 50 °C in a water bath. Then, an appropriate amount of FA was added, and the mixture was again attired for another 1 h. The resultant sol was allowed to age for 24 h. The precipitate was filtered, dried, and calcined at 120 °C for 2 h, forming Fe-TiO_2/FACs.

Meta-organic deposition (MOD)

The MOD approach is commonly used to make $BiVO_4$ nanocomposites [22]. The precursors are dissolved in a non-polar solvent, and the non-polar ligand covers the photocatalyst's polar centre. As a result, the resultant sample is very stable and water resistant [49]. Zhang et al. [22] examined the production of $BiVO_4$-coated fly ash cenospheres (FAC) for improved photocatalytic degradation efficiency. Typically, a solution of bismuth nitrate was prepared in acetic acid through stirring for 30 min. Another solution of vanadium tri-isopropoxide was prepared in acetylacetone. Both the solutions were mixed to obtain a Bi:V ratio of 1:1, and the resulting solution was stirred for 1 h at room temperature. Then, FACs were added to the above solution and stirred for another 3 h to obtain a homogenous mixture. The resulting precipitate was dried at 110 °C and calcined at 500 °C for 2 h to obtain the final product. Silane was used to modify the organofunctional properties of FAC's surface in order to facilitate the deposition of $BiVO_4$ film. Pt ions were added to the $BiVO_4$-FAC to boost efficiency [23].

Precipitation and Co-precipitation

This is a new approach for precipitating many components at once [62]. However, this method results in irregular morphology and particle size of the produced materials and often leads to impure materials [50–52]. Inorganic salts are precipitated by adding a stoichiometric amount of acid or alkali to the final solution, which is then heated in a small volume of oxygen to convert metal into metal oxides [66, 67]. Okte and Karamanis [37] prepared ZnO-FA for congo red (CR) degradation from an aqueous stream. Briefly, a solution of zinc nitrate was added into a solution of sodium carbonate and the predetermined amount of FA through magnetic stirring for 12 h. The precipitate was then centrifuged, dried and calcined at 500 °C for 5 h to obtain ZnO/FA nanocomposite. Further, Shaban et al. [53] synthesized a NiO_2-containing nanocomposite using the precipitation process.

Electrospinning

Electrospinning is a sophisticated method for creating nanofibers with diameters ranging from 10 nm to several micrometres [54]. A spinneret is used to pass the molten polymer through, and a high voltage is supplied in the solution. The molecules are charged, forming a hollow tube, and the solution evaporates as the voltage rises, leaving a solid nanofiber behind [55]. Saud et al. [56] reported the fabrication of TiO_2 nanofibers/FA nanocomposite by electrospinning method. Titanium precursor was mixed with acetic acid for 10 min, followed by the addition of appropriate amounts of polyvinyl alcohol, ethanol, and FA. The mixture was stirred for 6 h at room temperature before electrospinning at 15 kV. The resulting nanofibers were calcined at 600 °C for 3 h to obtain the final product.

Layer-by-layer assembly method (LBLA)

LBLA stands for layer-by-layer assembly method. Electrostatic attraction is used to coat the templates with thin films of opposite charges in this process. The salt solution is nebulized, followed by atomization. To obtain the final product, the residue was dried up and decomposed [57]. This process is utilized to produce oxide-based nanocomposites since it is easy and produces consistent film coating [58]. For instance, Cui et al. [59] reported the fabrication of $Ti_{0.91}O_2$/FA nanocomposite by the LBLA method. First, the FA is treated with polyethylenimine for 60 min through stirring to charge the FA surface negatively, and then, it is collected by centrifugation and dried. Then, a predetermined amount of negatively charged FA was mixed with a solution of $Ti_{0.91}O_2$ and stirred for 60 min. The resulting precipitate was washed with distilled water and dried before being treated with a poly(diallyldimethylammonium chloride) solution. The same process was repeated several times to obtain layered $Ti_{0.91}O_2$/FA nanocomposite.

Incipient impregnation approach

This method is cost-effective and straightforward, requiring no specific apparatus and producing no secondary pollutants. Fly ash nanocomposite can be impregnated with metal ions. Calcination can be used to reactivate the dried product [60, 61]. Xu et al. [62] extracted SBA-15 from FA and impregnated it with Co and Mn via an impregnation method. Typically, a known amount of SBA-15 was stirred with appropriate amounts of cobalt nitrate and manganese nitrate and the resultant solid mixture was collected, dried, and calcined at 500 °C for 2 h.

Green synthesis

There has been a rise in awareness over the past decades, and as a result, the need to employ green chemistry concepts has appeared in chemical research. Green synthesis methods have had a significant impact on the cost of nanomaterial production as well as pollution reduction. Natural products have been used to synthesize nanomaterials, which has helped to reduce costs and pollution. Proteins, cellulose, honey, and other natural products are readily available and inexpensive. During the preparation of nanomaterials, the natural compounds could be used as precursors, solvents, or surfactants. Natural products can effectively alter the size of particles and the shapes of nanoparticles due to their complex structure and characteristics. As a result, greater research into the role of these organic compounds in the green fabrication of nanoparticles is needed. Recently, Yadav et al. [63] utilized egg shells as a source of calcium to fabricate $CaMn_2O_4$/FA nanocomposite. The egg shells were washed and calcined at 800 °C for 4 h to obtain CaO. Then, appropriate amounts of CaO, manganese acetate, and FA were immersed in distilled water, followed by the addition of NaOH solution at constant stirring for 4 h at 80 °C. The precipitate was then washed, dried, and calcined at 550 °C for 2 h to obtain $CaMn_2O_4$/FA nanocomposite.

Because of its easiness, which does not necessarily involve the use of complex machinery or particularly high working temperatures, sol–gel is the most often used technique to synthesize metal oxide nanoparticles because the particles of desired morphology could be creased with some slight adjustments. The hydrothermal or solvothermal processes benefit from being a reliable approach, but they require high temperatures, and the particle size of the prepared composite may be altered by the temperature, reactant and solvent choices. The necessity for a costly hydrothermal autoclave, which demands extra safety procedures prior to usage, is one of the significant disadvantages. Precipitation and co-precipitation are innovative approaches that have the benefit of precipitating more than one component while allowing the particle size to be changed. However, the final product must be calcined and milled, which reduces the sample's purity [64]. Additionally, the green synthesis method is a trending research topic that involves using natural products to minimize the use of harmful chemicals during nanocomposite synthesis and helps minimize environmental pollution. Moreover, not much research has been conducted to investigate the green synthesis of fly ash-based nanocomposites and to understand the method of incorporating nanomaterials in fly ash. Thus, the green synthesis procedure should be motivated in future research.

Characterization and structure of fly ash nanocomposites

Fourier transform infrared spectroscopy (FTIR)

FTIR spectroscopy is an analysis technique for examining the characteristics of functional groups on the samples' surface, which is significant for the removal of contaminants in wastewater. The FTIR pictures of RHA and FACs-based nanocomposites are shown in Fig. 2. The presence of different functional groups and bonds could be depicted using FTIR. The O–H (3300–3000 cm^{-1}), H-OH (1692 cm^{-1}), Si–OH (1095 cm^{-1}), and Al–O–Si (600–500 cm^{-1}) bonds are easily identifiable in the FTIR spectrum of FA. After coating with the photocatalyst, the peak intensity associated with Si–O-Si and Al–O–Si in both rice husk ash and fly ash cenospheres diminishes, implying the development of novel functional groups amid FA-silica and photocatalysts [65].

X-Ray diffraction pattern

Figure 3 shows the X-Ray diffraction (XRD) peaks of RHA and FACs-based nanocomposites. The XRD pattern of RHA-10Sn [49, 68] has a strong peak at $2\Theta = 23.4°$. For TiO_2 and ZnO included RHA, a comparable peak was identified at $2\Theta = 23°$, confirming the occurrence of the amorphous nature of silica and crystalline phases of quartz in RHA-based photocatalysts [69]. The characteristics of RHA-10Sn were examined by Adam et al. [61], who discovered that the crystalline phase has no identifiable silica peak, signifying that Sn is evenly distributed over RHA.

All sharp diffraction peaks in the XRD pattern of TiO_2 integrated FACs (Fig. 3b) confirmed the existence of Mullite M ($3Al_2O_3{\cdot}2SiO_3$) and quartz Q, while a broad peak at $2\Theta = 24.0°$ suggested the existence of amorphous aluminosilicates in FACs [70]. The next peak in TiO_2-FAC at $2\Theta = 25.3°$ is of anatase, which is required to keep TiO_2 immobilized on FA and maintain the photocatalyst stability [71, 72]. The usual size of photocatalytic nanoparticles is believed to be between 10 and 30 nm [73].

Scanning electron microscopy (SEM)

Burning rice husk produces rice husk ash, which may be purchased cheaply from boilers that use rice husk for pore production [75]. RHA mostly comprises crystalline silica with no additional metallic oxides [76]. Figure 4 shows SEM images of raw RHA, acid-treated RHA, and base-treated RHA.

Raw RHA comprises finely structured crystal-like phases that resemble rolled-up peaks, as shown in Fig. 4a. Treatment of RHA with acid causes pores to develop on the

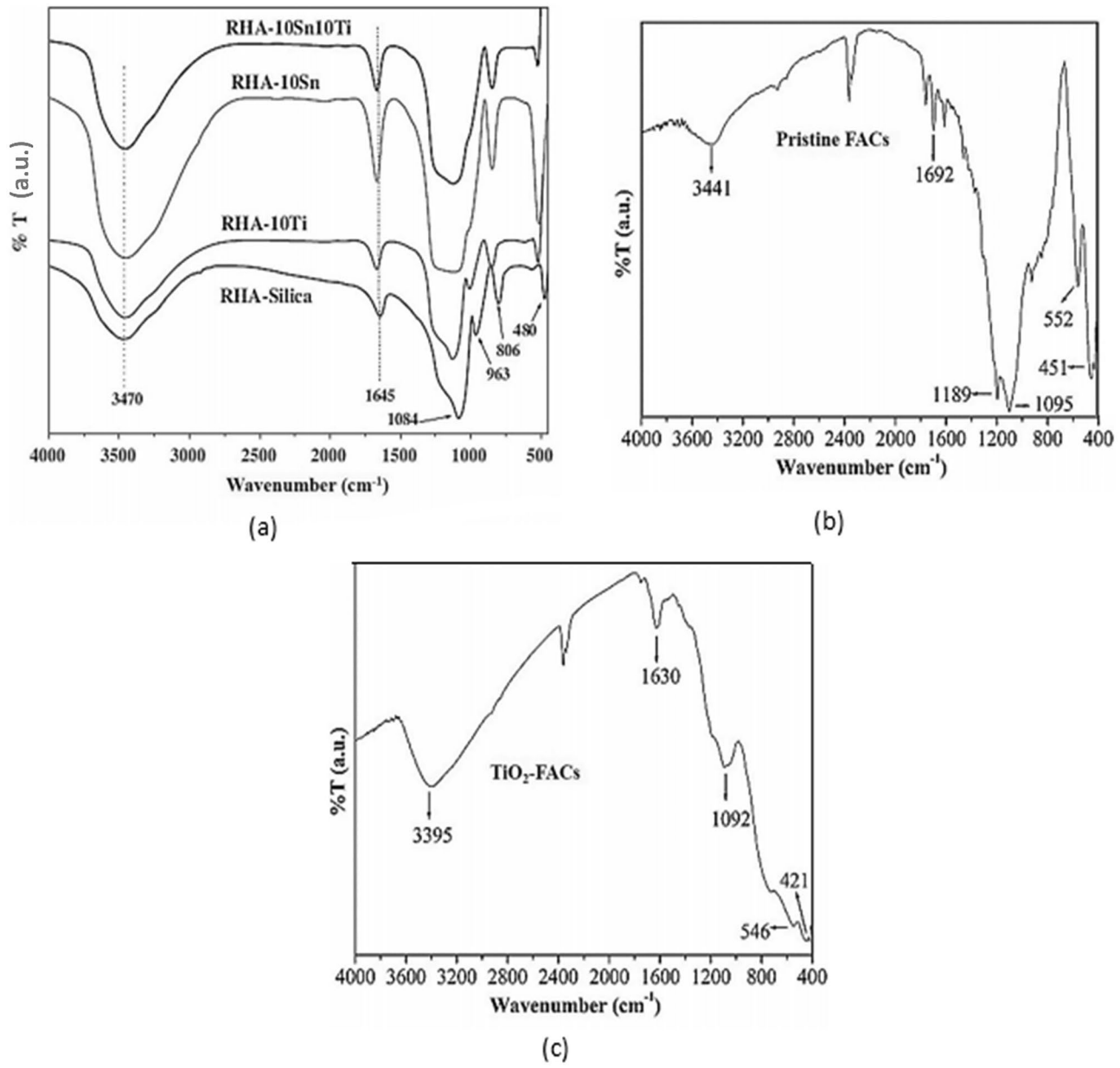

Fig. 2 FTIR images of (**a**) RHA-based photocatalysts [66], (**b**) Pure FACs, and (**c**) TiO_2-FACs [67]

surface of RHA because specific particles are fragmented as the surface is damaged (Fig. 4b). After alkali treatment, on the other hand, just a few pores remain [53, 77] (Fig. 4c). Figure 5 displays SEM images of TiO_2-RHA and RHA-10Sn photocatalysts, indicating that photocatalysts supported on rice husk ash are generally porous, with spherical and uniformly implanted photocatalyst particles on the RHA surface. The rough morphology of the treated RHA provides active sites for pollutant adsorption and a larger surface area, which increases the photocatalytic efficiency.

The structure of FACs is preserved throughout doping, and practically every photocatalyst has identical surface properties. During the coating of FACs with metal oxide layers, certain pores form on the surface, increasing adsorption efficacy [48, 80]. ZnO-FACs have a completely different morphology from TiO_2, $BiVO_4$, and CeO_2-supported FACs. It has a flower-like surface with clusters of various sizes [81].

Volcanic ashes (VA) are microscopic powdered particles generated from erupted volcanoes that were also used to support several photocatalysts [82]. Figure 6a depicts the morphology of raw VA's surface. VA is often made up of tiny prismatic porous assemblies of varying sizes ranging from a few nanometers to several micrometres [74]. As

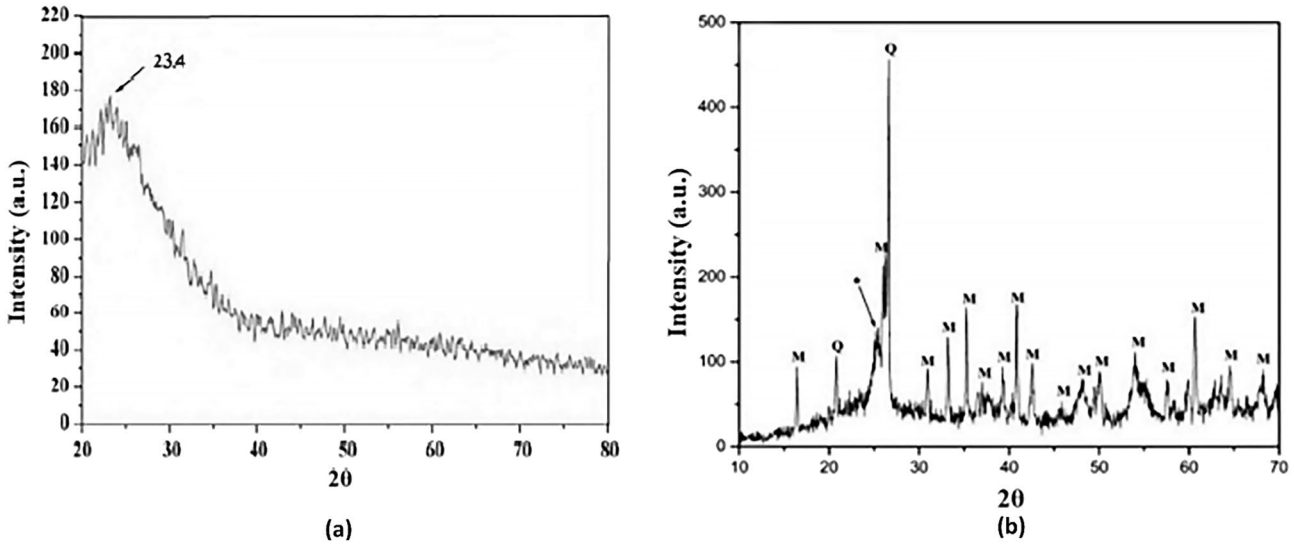

Fig. 3 XRD pattern of (**a**) RHA [74] and (**b**) FACs [70]-based photocatalysts

demonstrated in the SEM image of TiO_2-doped VA [70] and illustrated in Fig. 6b, doping has no major impact on surface morphology.

The morphology and characteristics of FA-based nanocomposites significantly affect the efficiency of the material because the reaction occurs entirely at the material's surface. Morphologies like nanosheets, nanoflowers, and nanofibers have a larger surface area, providing more active sites and increasing adsorption efficiency. The porous surfaces of rice husk ash, FACs, and VA provide more significant active sites for photocatalyst deposition and adsorption of contaminants [83]. Fly ash nanocomposites have a better surface-to-volume ratio due to their smaller particle size. This enhances the adsorption capacity of the nanocomposite while also increasing its photocatalytic efficiency by generating reactive oxygen species to boost the photodegradation of organic pollutants [22, 84]. Most of the photocatalysts showed a porous uniform spherical particle settled on the surface of FA. In the case of metal oxide nanocomposites, the SEM data show that the metal oxide films are evenly spread across the surface of fly ash particles.

Several studies reported highly stable photocatalysts, which show a removal efficiency of over 80% even after several successive cycles. It may be due to the fact that the structural integrity of the photocatalyst is maintained, and hence, the photocatalyst does not undergo photo-corrosion or decomposition easily. It is concluded that fly ash is an excellent adsorptive support to immobilize the photocatalyst on its surface to shield the surface-active sites against destruction, the synergistic contribution of adsorption, and generation of photogenerated reactive species for better photodegradation efficiency [85]. The decrease in the photodegradation efficiency after successive cycles is due to the change in mesoporous-microporous structure or decrease in the active sites due to leaching and lower stability of the photocatalyst [86].

Photodegradation of pollutants

Dyes have remained a significant water contaminant since their use in textile industries. Most organic dyes and other pollutants, including Cu, As, Cr, and Zn [87], are found in untreated textile waste and are known to cause diseases in animals and humans [88]. Some of the common dyes found in industrial wastewater include methylene blue, methyl orange, crystal violet, scarlet red, acid orange, acid red, and eosin Y. These dyes are non-biodegradable and raise the biological oxygen demand of the sample. Dyes block the sunlight from reaching the aquatic plants and hinder plant growth [89]. Dyes such as congo red, acid red 337, remazol black, and entrazole blue are carcinogenic [90]. Even low concentrations in the ppm range can form brightly coloured compounds in water, obstructing the photosynthesis process of underwater plants [91] and lowering the food-producing ability of aquatic plants [92, 93] by limiting sunlight from entering the water. Table 1 illustrates the performance of several FA-based materials for the photocatalytic degradation of organic pollutants.

While there are several strategies for removing dyes from wastewater, including adsorption, biodegradation, and coagulation, as well as a variety of effective adsorbents for dye adsorption, these processes do not break down dyes and move them to another phase, necessitating the use of additional treatment methods to avoid secondary pollution. As a result, researchers began looking for alternative strategies

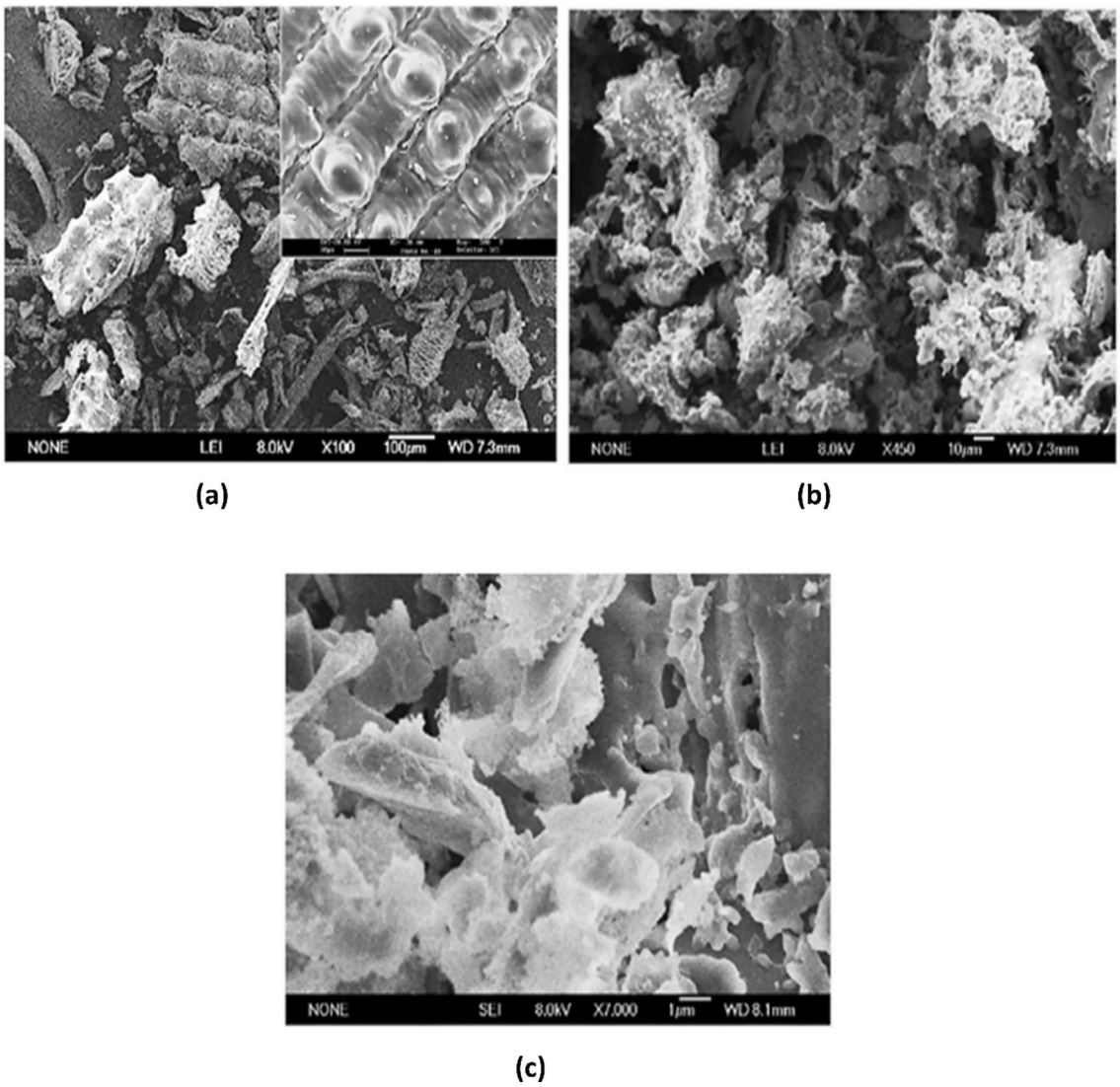

Fig. 4 SEM images of (**a**) raw RHA [77], (**b**) acid-treated RHA [78], and (**c**) alkali-treated RHA [53, 77]

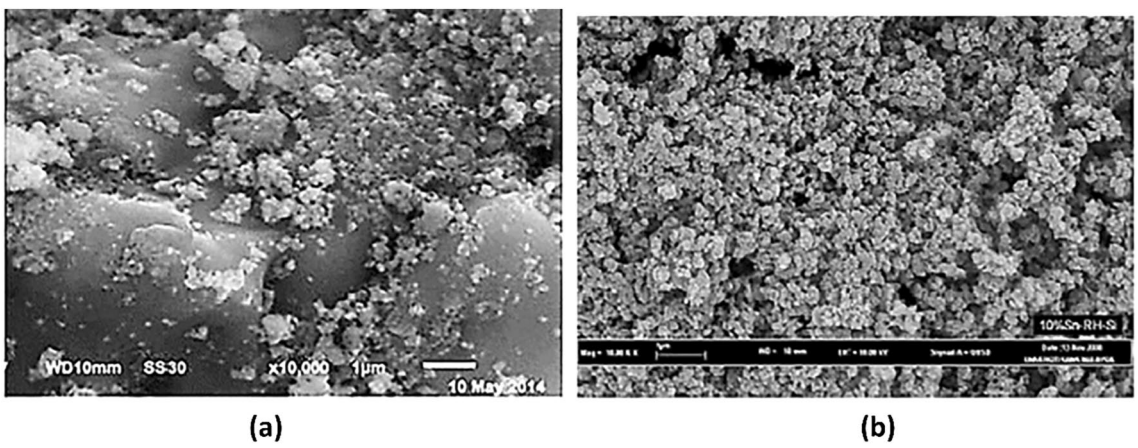

Fig. 5 SEM images of (**a**) TiO_2-RHA [77], and (**b**) RHA-10Sn [79]

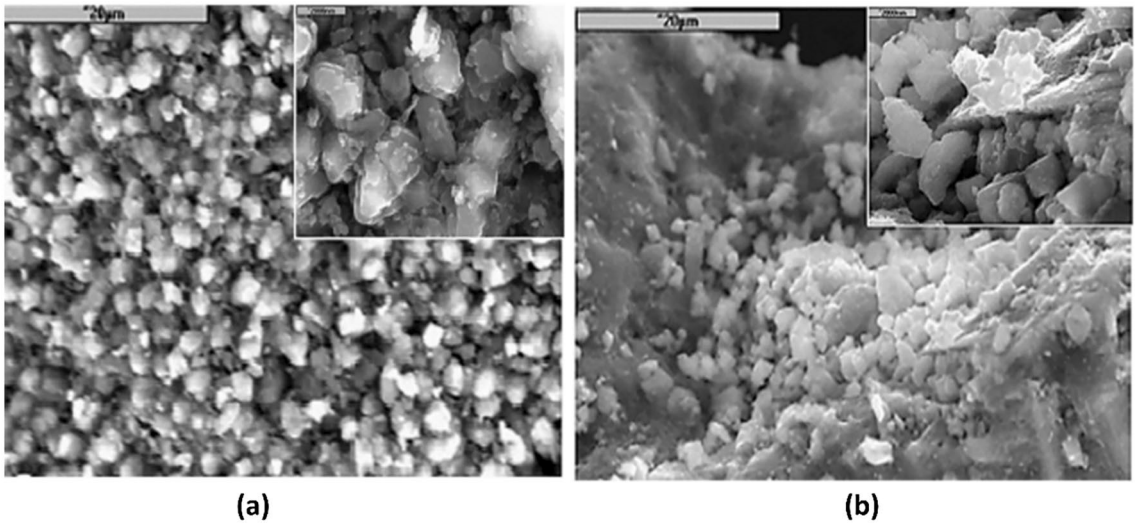

Fig. 6 SEM image of (**a**) raw VA [74] and (**b**) TiO_2-doped VA [70]

for degrading dyes into smaller compounds that do not cause secondary pollution. Researchers have developed a novel, improved oxidative method called photocatalysis for dye degradation that generates reactive oxygen species that oxidize dyes into CO_2 and H_2O [94–96].

Methylene blue (MB)

MB is a significantly hazardous dye that causes methemoglobinemia by the oxidation of haemoglobin (Hb) and reducing Hb's capacity to transport oxygen at higher dosages. Because of its easy degradability due to the presence of electronegative nitrogen atoms alongside sulphur atoms in the heterogeneous ring structure, it is used as a model dye to research dye photodegradation [97].

Cui et al. [59] examined the breakdown of methylene blue using $Ti_{0.91}O_2$-CFA produced using the LBLA technique and UV irradiation in a study. After 60 min, the dye concentration was lowered to half. Esparza et al. [82] found increased photodegradation effectiveness of TiO_2-VA. They examined the elimination of methylene blue under ultraviolet irradiation and at pH levels ranging from 3 to 10 using a hydrothermal approach to generate anatase TiO_2-impregnated VA nanocomposites. The findings revealed that 100% of the dye could be degraded within 30 min and that the photodegradation is unaffected by solution pH.

The degradation of MB in nitrogen-doped TiO_2-FACs produced by the sol–gel technique was investigated at various calcination temperatures [83]. The degrading efficiency of 25% N-TiO_2 is 10% greater than that of N-TiO_2/FACs and 40% higher than that of basic TiO_2-FACs. Furthermore, the materials calcined at higher temperatures resulted in improved photocatalytic performance.

CeO_2-doped fly ash cenospheres generated by the enhanced pyrolysis method were studied to degrade methylene blue from water samples under visible light [98]. Within 300 min of irradiation, 60% of the dye was eliminated, and the degradation followed first-order kinetics.

Wang et al. [48] evaluated the degradation efficiency of Fe-doped TiO_2-FACs synthesized by the sol–gel technique to pure TiO_2-FACs under visible light at various Fe^{3+} ion concentrations. The research reported that doping TiO_2-FACs with 0.01% Fe^{3+} ions boosts TiO_2 photocatalytic degradation effectiveness by 33%. Doping with Fe_2O_3 further improves photocatalytic efficiency [99]. The degradation of MB in Fe_2O_3–TiO_2/FACs was investigated under visible light. After 60 min of irradiation, the nanocomposites demonstrated an enhanced photodegradation efficiency of 86.81%. Furthermore, altering Fe_2O_3–TiO_2/FACs with hydrogen peroxide improved the photocatalytic efficiency even more. When compared to $Fe_2O_3TiO_2$/FACs, the improved FACs were 2.25 times more efficient. Huo et al. [100] also found that after modifying TiO_2-FACs with H_2O_2, the photocatalytic effectiveness increased by 42.5%, which can be exploited in practical applications.

The degradation of MB in pure $BiVO_4$, $BiVO_4$-FACs, and 2 wt % Pt@$BiVO_4$-FACs produced by the MOD technique was examined under visible light irradiation [22]. $BiVO_4$-FACs had a 2.5-fold greater photodegradation rate than pure $BiVO_4$. After 120 min of irradiation, $BiVO_4$-FACs degraded MB at a rate of 62%, while pure $BiVO_4$ degraded at a rate of 33% under similar conditions. Under identical conditions, doping $BiVO_4$-FACs with Platinum ions increased the degradation of methylene blue to 93%.

Kalpana and Selvaraj [101] used wet chemical synthesis to create amine-doped ZnS-Ag/FA to degrade methylene

Table 1 Photocatalysts with fly ash as a support

Dye pollutants	Photocatalyst used	Operating conditions				Removal efficiency (%) of FA supported photocatalyst	References
		Dye concentration (ppm)	Light source	Photocatalyst dosage (mg)	Photodegradation time (min)		
Rhodamine B	BiOBr/FACs	15	Visible	100	80	83	[64]
Rhodamine B	Fe/N-TiO_2-FA	8	Visible	200	240	81	[134]
Rhodamine B	Zn/TiO_2-RHA	0.47	Visible	25	100	95	[116]
Rhodamine B	AgCl/TiO_2/FACs	12.5	Visible	210	180	95	[117]
Methyl orange	TiO_2-LFA/H_2O_2	3.27	UV	200	30	79	[105]
Methyl orange	TiO_2-FA/H_2O_2	32.7	UV	400	300	90	[106]
Methyl orange	ZnO/FA	3.27	UV	100	10	100	[37]
Methyl orange	C–TiO_2/FA	20	Visible	100	90	99	[54]
Methyl orange	Cu-TiO_2	10	UV	–	30	100	[107]
Methyl orange	PPY/Fe_3O_4-FA	10	Visible	100	240	78.8	[109]
Methyl orange	g-C_3N_4/N–TiO_2/FACs	20	Visible	300	180	72.2	[111]
Methyl orange	$BiVO_4$/FACs	10	Visible	200	360	82.2	[110]
Methyl orange	S,N,Co/TiO_2/FMS	20	Visible	200	60	65	[20]
Methylene blue	N/TiO_2-FACs	20	Visible	1800	540	58	[98]
Methylene blue	Fe/TiO_2-FACs 0.01%	20	Visible	1800	–	50	[48]
Methylene blue	Fe_2O_3/TiO_2-FACs/H_2O_2	2	Visible	100	60	86	[99]
Methylene blue	$BiVO_4$-FACs	10	Visible	200	300	90	[22]
Methylene blue	ZnS/A-FA 3%	12	UV	50	90	100	[101]
Methylene blue	RHA-10Sn10Ti	12	UV	20	240	99	[68]
Methylene blue	TiO_2 nanofibers	10	UV	20	120	100	[56]
Methylene blue	FA geopolymer	1.3	UV	200	30	92.79	[103]
Methylene blue	TiO_2-RHA zeolite	20	UV	100	180	99.4	[104]
Methylene blue	Pt–BiVO4/FACs	10	Visible	200	120	93	[23]
Methylene blue	ZnO-FA polymer	10	UV	15	120	100	[81]
Indigo carmine	GR-FAG	10	Visible	100	90	90	[121]
Acid red 1	Co-LFA	10	Visible	100	60	99	[112]
Bemacid rot	TiO_2-FA	30	UV	500	120	90	[113]
Bemacid Blau	TiO_2-FA	30	UV	500	240	90	[113]
Congo red	Ni_2O_3/MCM-48 (RHA)	5	Visible	20	360	94	[53]
Brilliant green	CeO_2/Zeo/NaX	10	Visible	100	180	100	[118]
Reactive Red 45	TiO_2-FA	30	UV	100	90	90	[114]
Sky blue 5B	Mn/CuO-GR-FAG	20	UV	100	100	100	[120]

blue under UV radiation at various pH levels and investigate its antibacterial capabilities. The dye was completely removed in 90 min, according to the research. The reaction is pH dependent, with a pH of 9 achieving optimal efficiency. In addition, ZnS-Ag/FA is particularly effective against *S. Aureus* and *E. Coli* elimination.

Adam et al. [68] synthesized several Sn- and Ti-loaded RHA nanocomposites and examined the photodegradation of MB from water samples under various pH levels. The photodegradation efficiency of RHA-10Sn10Ti was almost 100%, per the pseudo-second-order kinetic model. At pH 4, the degradation efficiency rose to 88%, up from 54% at pH 2, and the reaction was pH-dependent. Furthermore, the maximum efficiency was obtained at higher pH; above pH 10, the removal efficiency was nearly constant. The results are comparable to those of El Qada et al. [102], who determined the optimal pH to be 11. Sauda et al. [56] attempted to evaluate the removal of MB using TiO_2-FA nanofibers produced by electrospinning. After 2 h of UV light irradiation, complete degradation of MB was accomplished.

Zhang and Liu [103] studied the photocatalytic degradation of MB under UV irradiation using a fly ash geopolymer having a typical pore diameter of 50 nm, and outstanding degradation efficiency of about 93% was attained owing to the synergistic effect of adsorption and photodegradation. Although the adsorption results matched

pseudo-second-order kinetics, MB degradation followed third-order kinetics. The degradation efficiency is depicted in Fig. 7 under different conditions.

The ability of TiO_2-impregnated zeolite to remove MB from water samples and the outcome were compared to anatase phase TiO_2 [104]. In the case of TiO_2-zeolites, the highest removal efficiency was found to be 99.4% in a short span of 30 min, while only 82% photocatalytic efficiency was achieved after three hours with anatase TiO_2 under visible light. The UV–visible spectrum of photodegradation of MB employing anatase and zeolite is shown in Fig. 8 [104]. The authors discovered that doping photocatalysts with Fe, N, and Sn using polyethylene glycol as a surface activating and capping agent could significantly increase photodegradation performance.

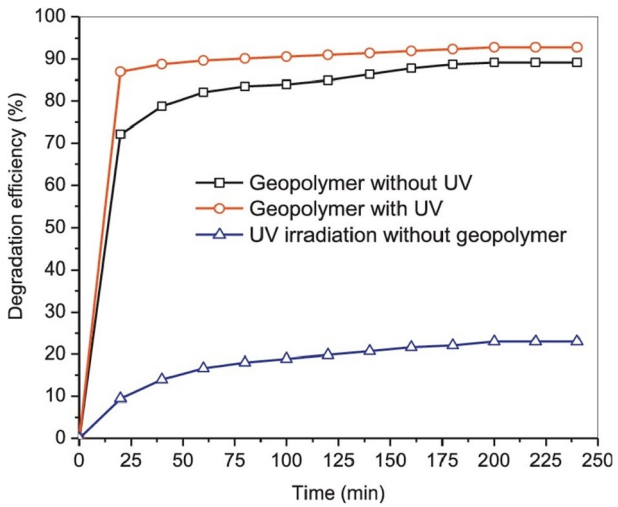

Fig. 7 MB photodegradation efficiency at various conditions (Reproduced with permission from Elsevier) [103]

Methyl orange (MO)

MO is a typical volumetric analysis indicator that can cause serious gastrointestinal upset if consumed. Several researchers investigated the photodegradation of MO using FA-based nanocomposites.

Okte and Karamanis [105] examined the photodegradation of MO under UV irradiation using TiO_2 anchored on lignite prepared by using the sol–gel method. The findings showed that the reaction was following pseudo-first-order (PFO) kinetics, with around 50% of the original dye concentration degrading after half an hour of irradiation with 25% TiO_2-FA. Under comparable conditions, further activating the photocatalyst with H_2O_2 reduced the original dye concentration to almost 80% in 30 min. Similar findings were reported by Visa and Duta [106], who found that after modifying TiO_2-FA with H_2O_2, the degrading efficiency of methyl orange could be increased to over 90% just after 300 min. Furthermore, Okte and Karamanis [37] prepared ZnO-FA nanocomposites after a year to evaluate MO photodegradation. Within 10 min of ultra-violet irradiation, the photocatalyst demonstrated outstanding photodegradation efficiency of around 100%.

An et al. [54] examined the photodegradation of MO in carbon-doped TiO_2-FA under UV irradiation, and the results exhibited that almost 100% of the 20 ppm dye could be removed within 90 min of irradiation. Kanakaraju et al. [107] used the sol–gel technique to synthesize Cu-doped, base-modified TiO_2-FA. They examined the photodegradation of methyl orange under UV and Visible light irradiation to improve the degradation efficiency of TiO_2-FA. The unique photocatalyst effectively degraded 100% and about 99% of the dye in UV and visible light radiation in just 30 min while maintaining the initial dye concentration of 10 ppm. The photodegradation efficacy of TiO_2-FA could be improved by

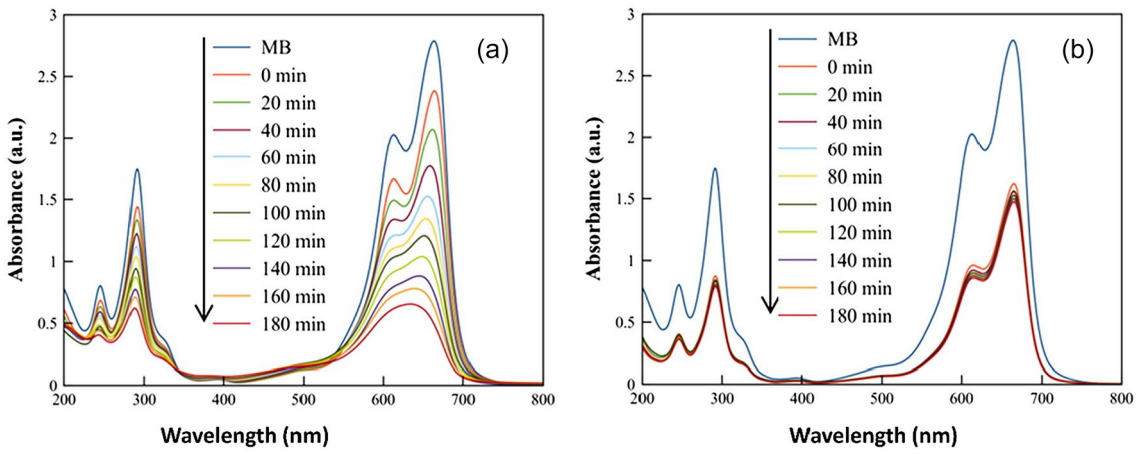

Fig. 8 UV–visible spectrum of MB in (**a**) anatase TiO_2 and (**b**) TiO_2-zeolite with respect to irradiation time (Reproduced with permission from Elsevier) [104]

doping with transition metals such as phosphorous (1%) and molybdenum (1%); the photocatalyst shows enhanced activity in visible light irradiation owing to a decreased bandgap energy from 3.29 of pure TiO_2 to 3.20 for P/Mo co-doped TiO_2 [108].

The photodegradation of MO employing Fe_3O_4 nanoparticles anchored on polypyrrole and FA produced via the sol–gel technique was investigated in visible light irradiation [109]. The photodegradation efficacy of PPY/Fe_3O_4-FA was determined to be about 79% in 4 h. The degradation of MO in novel $BiVO_4$-FACs generated by the MOD technique was also investigated under visible light. It had an 82% photodegradation efficiency after 360 min of irradiation, but pure $BiVO_4$ showed only 40% degradation efficiency [110]. Zhao et al. [111] examined the photodegradation properties of a ternary nanocomposite of g-C_3N_4/N-TiO_2/FACs for the degradation of methyl orange, and the degradation efficacy was compared to that of N-TiO_2-FACs and pristine g-C_3N_4. The results revealed that g-C_3N_4/N-TiO_2/FACs could degrade almost 72% of MO after 180 min, which is 1.3 times more than N-TiO_2-FACs and about 3.5 times greater than g-C_3N_4.

Other dyes

Under UV irradiation, Giribabu and Swaminathan [112] investigated the photodegradation of Acid Red 1 (AR1) from wastewater using cobalt-doped lignite fly ash. At an ideal pH of 2.5, the photocatalyst was successful in eliminating 99% of the dye in 60 min. The process is a pseudo-first-order reaction, according to kinetics research. Under UV irradiation, Visa and Duta [113] investigated TiO_2-FA for degrading Bemacid Blau (BB) and Bemacid Rot (BR). The material demonstrated outstanding degradation efficacy of nearly 90% after 2 h for BR and 4 h for BB. Due to its larger size, BB takes a long time to degrade as compared to BR. Gilja et al. [114] examined the degradation of Reactive Red 45 by irradiating it under ultraviolet light using TiO_2-FA. The photocatalyst exhibited the maximum photocatalytic efficiency of 90% after 90 min at pH 3. Wang et al. [115] examined the photodegradation of rhodamine Blue (RhB) and Reactive Brilliant Blue KN-R using nitrogen and iron-doped TiO_2 on FA-forming adsorbent (FFA) synthesized via the sol–gel technique. The photodegradation of KN-R and rhodamine B is pseudo-first order, with the Langmuir model best fitting the adsorption data. At a pH of 4, the photocatalyst effectively degraded about 97% of KN-R after 1 h of UV light irradiation and roughly 80% of RhB after 4 h under visible light.

Chen et al. [116] examined the photodegradation of RhB using floating zinc- and nitrogeṇ-doped TiO_2 calcium silicates (ZTRH) nanocomposites prepared via the sol–gel technique and exposed to visible light. In under 100 min, ZTRH was able to degrade roughly 95% of RhB. The photodegradation of RhB was also examined in floating FACs-supported AgCl-TiO_2 films [117]. Under visible light irradiation, the photocatalyst was able to remove nearly 95% of the dye in about 180 min. Lin et al. [64] used FACs to support BiOBr/BiOI photocatalysts and examined the degradation of RhB underneath visible blue light to improve the photodegradation efficacy of FACs. Within 30 min, 99% removal efficiency can be reached. Shaban et al. [53] examined the elimination of CR dye using MCM-48/Ni_2O_3-RHA produced via precipitation. The photocatalyst successfully eliminated 94.1% of the dye while maintaining the initial concentration of 5 ppm.

The degradation of Brilliant Green (BG) was investigated using CeO_2-supported CFA zeolite NaX (CeO_2/Zeo-NaX) [118]. About 100% of 10 ppm dye could be degraded at pH 10. Zhang et al. [119] were the first to inspect the degradation of dyes from water samples by graphene-loaded geopolymer (GR-FAG). Sky Blue 5B degradation was investigated using manganese-doped copper oxide-loaded GR-FAG. Under visible light, the photocatalyst could remove 100% of the dye. Zhang et al. [120] examined the utilization of graphene-loaded geopolymer to remove Indigo Carmine, the most extensively used dye in the textile industry. 1.0GR-FAG eliminated around 90% of the initial dye concentration under visible light.

Other organic compounds

Various organic and pharmaceutical pollutants in industrial effluents include phenols, bisphenol A (BPA), oxytetracycline, and other dyes. Under UV–visible irradiation, FACs degrade these compounds with an efficiency of more than 80% for the majority of pollutants.

Sun and Zhang [110] evaluated the influence of H_2O_2 on the degradation efficiency of $BiVO_4$-FACs (BFACs) for the photodegradation of phenol. Within 150 min, BFACs exhibited a 20% deterioration rate of 15% greater than pure $BiVO_4$ under visible light. However, after adding 1 mmol/L of H_2O_2, the degradation rate increased significantly to 78% in 150 min. The degradation of BPA using 1:3 polypyrrole (PPY)-Fe2O3/FACs was reported by Dagar and Narula [109]. Within 240 min, the photocatalyst achieved the maximum degrading efficiency of 75%.

Lu et al. [121] conducted a unique investigation of the degradation of enrofloxacin from water samples employing magnetic floating FACs. The degradation rate could reach up to 75% in 1 h of visible light. Furthermore, the authors also investigated the degradation of tetracycline (TC) [122] in multi-antibiotic solutions containing oxytetracycline (OTC) and ciprofloxacin (CIP) employing poly-o-phenylenediamine (POPD)/TiO_2/FACs as supporting material for molecularly imprinted photocatalyst (MIP). The photodegradation rate of TC under visible light could reach 77%.

The photodegradation rate of tetracycline was determined to be 3.3 min^{-1} in a multi-pollutant system, demonstrating that the prepared photocatalyst has robust selectivity and high efficiency in degrading tetracycline in the aqueous form.

Factors affecting degradation of dyes

Light source

The degradation efficacy is determined by the photocatalyst's bandgap and the irradiation source [101]. When photocatalysts with a broader energy gap are irradiated with UV light, they have a much better degradation efficiency, whereas photocatalysts with a lesser bandgap need visible light irradiation [123]. Many studies are still underway in this field, intending to lower the energy gap of photocatalytic nanocomposites such that increased photodegradation efficacy can be achieved by doping with other elements. When exposed to visible light, Coronado et al. [66] successfully prepared CeO2-FACs for improved photocatalytic activity. Because of the presence of fly ash, the bandgap is somewhat pushed towards the visible range between 450 and 800 nm, improving the photocatalytic activity compared to pristine CeO_2.

The solution pH

The pH of a solution has an important impact on the formation of intermediate radicals and dye ionization [124]. The generation of $OH^{\cdot}$ radicals, the ionization of dyes, and the physicochemical properties of the dyes are largely affected by the solution's pH. Depending on the pH, the dyes may be cationic, anionic or neutral in an aqueous medium. Therefore, the pH range for photocatalytic degradation depends on the dyes and photocatalytic nanocomposite with respect to pK_a values and the theory of zero-point charge; therefore, some photocatalytic reactions show pH dependence [125]. According to Peng et al. [126], anionic dyes are quickly photodegraded at lower pH, but cationic dyes comparatively require a higher pH to degrade. A rise in the pH of the solution from 3 to 9 enhanced MB degradation, but photodegradation efficiency decreased by increasing pH. The surface of the photocatalyst becomes positively charged at lower pH, resulting in electrostatic repulsions between dye cations and photocatalyst, thereby reducing the adsorption capacity. Protons also compete along with dye-cations for adsorption on the photocatalyst surface at lower pH [101]. The photocatalyst's surface becomes negatively charged when the pH of the solution rises, increasing electrostatic attraction towards the dye cations and thereby enhancing dye adsorption and photodegradation capacity. Furthermore, at greater pH, the availability of OH^- ions is greater, causing more holes to react with them, resulting in the production of OH^- radicals. However, beyond pH 11, the photodegradation efficiency drops because the OH^- radicals are adsorbed by the dyes on the photocatalyst surface.

Initial concentration of dye

With a constant time of irradiation, the influence of initial dye concentration on photocatalyst degradation efficiency was examined. A higher dye concentration was associated with a decreased degradation efficiency in most cases [94]. This is because, at increasing dye concentrations, the photocatalyst's surface becomes saturated with the dyes, inhibiting the generation of $OH^{\cdot}$ radicals and lowering the photodegradation efficacy [95, 101]. Similarly, a greater initial dye concentration limits reactive sites on the photocatalyst surfaces, resulting in an extended contact time for an identical amount of dye degradation at a lower initial dye concentration. The intermediate ions formed during a photocatalytic process disperse gradually on the surface of the photocatalyst, deactivating the active surface sites, according to Ren et al. [96]. Furthermore, increasing the initial dye concentration causes the reaction mixture to become opaque, favouring light scattering and reducing the photocatalyst's light-harvesting property, lowering photodegradation efficiency [127]. Further, Mishra et al. [128] reported that higher dye concentration often leads to photolysis rather than photocatalysis, slowing the reaction rate. The degradation efficiency of rose Bengal dye declined after increasing the initial concentration [129]. The degradation slumped to 96.2% when the dye concentration increased from 5 to 200 ppm. The decrease was attributed to the increased opacity of the solution and the blockage of the photocatalyst's active sites, which reduced ROS production.

Photocatalyst loading

The effect of photocatalyst loading must be investigated since it significantly impacts the cost and applicability of photocatalysts in industrial applications. Esparza et al. [82] looked at the effect of photocatalyst concentrations ranging from 0.5 to 20 ppm on MB degradation. The research reveals that as the concentration of photocatalysts increases, so does the degradation efficiency. The results were in accordance with Wang et al. [43] for the discolouration of MB using platinum-doped TiO_2-FAC. The rise in degradation efficiency with increasing photocatalyst concentration is attributed to an increase in the number of active sites, which boosts adsorption efficiency and improves the light-harvesting properties, resulting in the generation of reactive oxygen species, improving the photocatalytic process [130].

On the other hand, Begum et al. [131] found that the degrading efficiency remained constant after an optimal

photocatalyst concentration. In addition, if the photocatalyst concentration is raised above a certain point, the photocatalyst begins to agglomerate, reducing the transparency of the solution and, as a result, reducing the amount of light reaching the photocatalyst [131]. A reduction in light absorption reduces the creation of OH^- radicals, which impacts the production of superoxide radicals, lowering the reaction's degradation rate [91]. Thus, employing the photocatalyst in the right proportion is critical to reducing internal collisions between photocatalyst molecules [132].

Calcination temperature

Calcination temperature significantly impacts a photocatalyst's dye degrading efficiency. Because temperature affects the morphology and size of TiO_2, the photodegradation performance of TiO_2-doped FA based is substantially determined by the calcination temperature. Li et al. [98] developed nitrogen-doped TiO_2-FACs and investigated the effect on photodegradation efficiency for MB degradation at various calcination temperatures. The results showed that as the calcination temperature rose to 450 °C, the photodegradation efficiency increased while the rate of photodegradation declined above this temperature. Another study by Zhu and Wang [133] found that beyond 350 °C, titanium dioxide transformed into amorphous anatase, increasing the photocatalyst's degrading efficiency.

The decline in the photodegradation efficiency beyond 650 °C was due to the development of larger-sized rutile TiO_2, which increased the energy gap [56, 135]. Based on these findings, the optimum calcination temperature for TiO_2 nanocomposites was set at 300–400 °C.

Mechanism of dye degradation

Ökte and Karamanis [105] proposed a schematic diagram of the mechanism for the photodegradation of methylene blue (MB) dye by fly ash-supported TiO_2 photocatalyst. When TiO_2 is immobilized over FA support, the dye molecules that are adsorbed on the surface of FA are spontaneously transferred to the surface of the TiO_2. The photocatalyst gets excited when the light of energy greater than the bandgap energy of the photocatalyst is incident on the photocatalyst. The mechanism of methylene blue (MB) degradation as a model dye using TiO_2-fly ash is shown in Fig. 9. The photocatalytic efficiency depends upon the dye concentration, surface area of nanocomposite and target contaminant, the angle of contact, and the percentage loading of photocatalyst on FA [136]. TiO_2 is anchored on FA, which aids MB adsorption and raises the dye concentration on the TiO_2 surface and thus FA enhances the photocatalytic activity of the photocatalyst. When the light energy (hv) larger than the energy gap 3.2 eV is used to activate TiO_2, the transfer of photogenerated electrons from the valance band (VB) to the conduction band (CB) occurs, which generates a positive hole in CB [137]. The electrons react with the trapped oxygen molecules on the TiO_2 surface, forming peroxide radicals that react with adsorbed dye molecules.

On the contrary, holes in the CB oxidize MB, forming hydroxyl radicals upon interaction with adsorbed water molecules. FA also aids in the retention of free radicals on its surfaces, enhancing the pace of MB breakdown on the TiO_2 surface [138]. Finally, the photocatalyst produces a sequence of reactive radicals that decompose the dye into CO_2, H_2O and other reduced molecules [43]. The increased degradation efficiency was attributed to the synergistic effect of the photocatalyst's combined adsorption on fly ash and photodegradation [138].

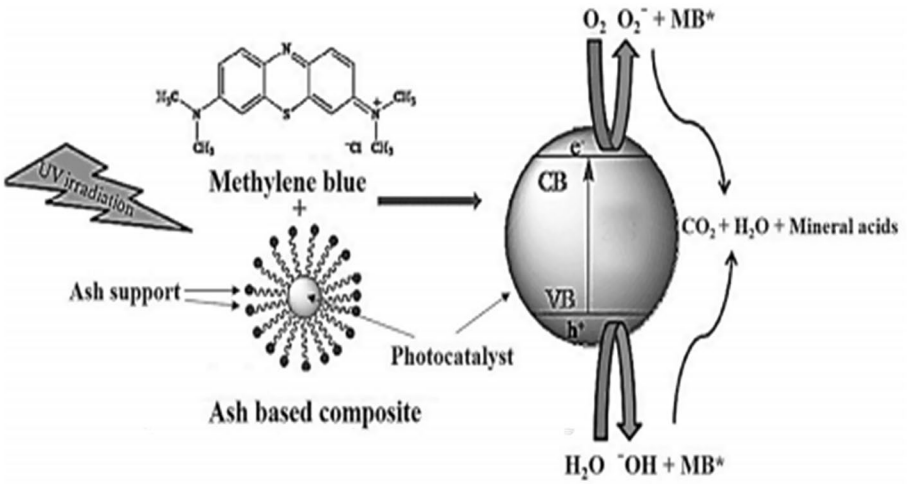

Fig. 9 Schematic diagram of the MB degradation mechanism by TiO_2 supported on FA [105]

Reusability and stability of fly ash photocatalysts

It is critical to prevent secondary pollution by renewing and reusing the material, lowering treatment costs, and saving resources. Fly ash is waste material, and utilizing waste material for useful purposes such as environmental remediation will add value to the waste product. It will be cost-effective compared to commercial catalysts. Moreover, FA nanocomposites are highly reusable, which further reduces treatment costs. As a result, it is essential to evaluate the prepared photocatalyst's stability. After the initial treatment, the nanocomposites are utilized in another process. Photocatalyst regeneration methods include acid washing, filtration, and washing [98]. Calcination is another efficient way of maintaining photocatalytic activity that can be used in conjunction with other regeneration techniques. A high calcination temperature causes the adsorbed materials to burn, which reopens the pores and regenerates the catalyst [105]. Hence, it becomes necessary to investigate the safety factor of the synthesized photocatalyst for cost-effectiveness. The prepared nanocomposite photocatalyst is filtered, dried, and reused for several cycles after the first treatment. The literature suggests that the prepared ash-based photocatalysts can be reused for a few successive cycles. Further, calcination could be an additional step, followed by other regeneration techniques to maintain the photocatalytic efficiency of the nanocomposites. According to the literature, the calcination temperature varied within the range of 400–500 °C to remove the pollutants accumulated within the cavities and active sites of the photocatalysts [43].

According to the literature, studies claim high stability and reusability of the fly ash nanocomposites [22, 43, 85]. This can be attributed to the fact that once the structural integrity of the photocatalyst is preserved, the photocatalyst cannot be easily corroded or deactivated during a photocatalytic reaction. Additionally, ash could be used as a support to anchor and stabilize the dispersion of photocatalysts onto the adsorbent surface, protecting the surface binding and catalytic sites from degradation. The combined effect of adsorption over fly ash and the generation of photoinduced charges caused the degradation of contaminants. However, a slight decrease in the photocatalytic activity after a few cycles could be due to the disruption of the microporous structure of fly ash and the reduction in the surface-active sites.

Removal of air contaminants

FA's high porosity, large surface area, suitable pore size, and other properties make it an inexpensive adsorbent that may efficiently reduce environmental pollutants through simpler processing [139]. Various reports analyse the applicability of fly ash and its nanocomposites for removing toxic gases from the environment. This section briefly discusses the utilization of FA and its adsorbents for the sequestration of gas contaminants from the air.

Removal of volatile organics

Volatile organic compounds (VOC) are a class of organic hydrocarbons that are generally produced as the byproduct of the combustion of fossil fuels, paint, refining, and other chemical manufacturing industries [140–142]. Anthropogenic volatile organic compounds have dramatically increased during the past few decades as a result of the industry's rapid development. These organic gases have more than 300 chemical forms, including alkanes, aromatics, esters, and aldehydes [143]. Several compounds, including the probable carcinogens benzenes and formaldehyde, are toxic to people at even trace levels [144]. The paint industry is the largest producer of xylene and aliphatic hydrocarbons, both hazardous to the ecosystem [145]. Ozone, peroxide, nitro-aldehydes, and other photochemical smog chemicals are produced in sunlight by photochemical interactions between VOCs and NOx, harming human health and causing secondary pollution. These compounds also have an adverse effect on the respiratory system and eyes. It was also claimed that fly ash removed several gaseous organics. Unfortunately, relatively few studies on eliminating volatile organic compounds using FA were documented in the literature. Successfully synthesizing polyurethane fibres with various concentrations of FA, Kim et al. [146] examined the adsorption of chloroform, benzene, toluene, xylene, and styrene on these fibres. They discovered that polyurethane fibres with 30 wt% FA had the lowest fibre diameter and the greatest SSA compared to other fibrous membranes. This led to the highest sorption capability. Moreover, the sequence of the following VOCs adsorbed by fibrous membranes was styrene > xylene > toluene > benzene > chloroform. This is because the adsorption of volatile organics is affected by several factors in addition to SSA and fibre diameters, such as polarity, chemical structure, morphology, pore size, presence of functional groups, electronic and steric effects, and temperature [147, 148]. Due to their instability, aromatic chemicals with lower ionization potential are typically simpler to absorb by FA fibre membranes [149].

Fly ash was used by Peloso et al. [150] to remove toluene fumes from the air. In order to evaluate the impact of some geometric, physical, and chemical characteristics of FA on toluene recoveries, the sorption of toluene vapours on FA has been specifically studied. The impact of particle accumulation and chemical activation on total porosity, the sorbent's SSA, and the adsorption phenomena suggested that fly ash products might be produced with an acceptable level of sorption performance. Fly ash that has been thermally

activated showed similar good results for toluene vapour adsorption [151]. The pyrolysis created a liquid oily fraction with good calorific value, a gas with a high hydrogen content, and a carbonaceous dry matrix with favourable microstructural features. It was then put to use for the successful adsorption of toluene vapour [152]. Rotenberg et al. [153] reported the adsorption of aromatic hydrocarbons and m-xylene on FA and reported the adsorption kinetics. The adsorption mechanism involved the intercalation of gases into the pores of FA. Further isotherm studies revealed that the adsorption efficiency does not depend on the temperature. However, the adsorption rate reduces with increasing vapour pressure. They proposed that the diffusion process governed the adsorption process.

Eiceman [154] looked into the adsorption of polycyclic aromatic hydrocarbons (PAH) on FA and found that adsorption is quick, isotherms are nonlinear, and irreversible adsorption happens at concentrations lower than 30 µg PAH/g fly ash. However, The adsorption methods for PAH are essentially controlled by vapour pressures at concentrations higher than 30 µg/g. Using an HPLC method, the adsorption of PAHs on diverse FA samples from burning Australian bituminous and brown coals was investigated [155]. The Freundlich equation can best capture the sorption data according to analyses of a number of standard isotherms. According to a correlation analysis between fly ashes' physiochemical features and PAHs' adsorption capacity, the residual carbon content is the key regulating factor. Recently, Liu et al. [156] investigated the synthesis of CeO_2/MnO_2-supported organic acid ligand-treated FA (Ce-Mn-OFA) for removing volatile organics. For benzene, toluene, m-xylene, and ethylene, the Ce-Mn-OFA catalyst had the maximum catalytic activity, reaching 90% conversion at 283 °C, 237 °C, 216 °C, and 264 °C, respectively. The ensuing modifications to the fly ash characteristics significantly increased Ce-Mn-oxidation OFAs and adsorption activity, increasing the catalyst's capacity for volatile organic compound removal. Reports suggest that the incorporation of MnO_2 into FA through ball milling caused an increased SSA and high catalytic efficiency, reaching more than 90% towards the removal and oxidation of toluene [157].

Removal of oxides of nitrogen

The occurrence of unburned carbon content and properties, such as its high porosity and high SSA of FA, can adsorb a small quantity of NOx [158]. This carbon is a precursor to AC, but during combustion in a power plant furnace, it underwent devolatilization [159]. As a result, the FA can be easily modified to activate the internal carbon, increasing its adsorption capability. The optimal approach for activating carbon is chemical demineralization, which is generally employed in combination with methods like activation by steam and physical separation since fly ash enriched with carbon contains a high amount of ash [160]. In their study on the adsorption of NOx by unburned carbon from FA, Rubio et al. [160] discovered that after 10 h, the conversion curves of NO on various FA samples achieved a steady state. Due to its higher carbon content, surface area, and porosity, the enriched-carbon FA also demonstrated strong NO abatement capability. For the purpose of removing NOx from flue gas, Izquierdo et al. [12] synthesized Cu and Fe exchange type Y zeolites from FA. According to Rubel et al. [161], carbon-rich combustion ash products may reduce NOx and Hg emissions as a result of ion-pair interaction between NO^+ and O_2^- at the surface of the carbon, which leads to the condensation of NO_2 in micropores. Also, after a certain quantity of Hg is adsorbed, it changes the pore surface of the adsorbent materials, generating the ideal pore size for adsorbing NOx [162]. Moreover, Rubel et al. [161] demonstrated that the adsorption of NOx enhanced the surface area of adsorbents.

NO elimination has also been done using AC made from unburned carbon found in CFA [163]. It was noted that in order to create AC that is more suitable for environmental remediation applications in the gaseous phase, the mineral matter must be properly removed from unburned carbon in fly ash prior to activation. Fly ashes were mechanically sieved to get the carbon-rich fraction, and the mineral content was then demineralized using the standard methods of HCl and HF. The sample was activated using steam at a temperature of 900 °C in order to increase pore size. A novel material for the adsorption of NO by ammonia employing AC as a sorbent at low temperatures was carried out in order to examine the usage of unburned carbon as a raw material for the manufacture of AC for the remediation of flue gas.

Another study investigated the effect of injecting FA into the discharge region on NO elimination [164]. Several combinations of NO, N_2, O_2, and with and without water vapour were combined with fly ash. Many studies have been conducted on NO elimination techniques utilizing nonthermal plasma chemical processes. Investigations were also conducted to see how adding fly ash might affect the elimination of NO utilizing short-pulsed discharge plasmas. The use of four distinct gas mixtures:

$$N_2 + NO \quad (1)$$

$$N_2 + NO + O_2 \quad (2)$$

$$N_2 + NO + H_2O \quad (3)$$

$$N_2 + NO + O_2 + H_2O \quad (4)$$

-in the presence and absence of fly ash was explored [165, 166]. Fly ash was used to investigate the NO ($NO + NO_2$) removal because it applies to actual circumstances in

coal-powered thermal power plants. Fly ash was present, and while it somewhat decreased the NO removal rate for dry gas combinations, it significantly boosted the NO removal rate for wet gas mixtures. The elimination of NOx from flue gases released by thermal power plants is said to benefit from the inclusion of fly ash, which also contributes a small amount of moisture to the mixture [167].

Furthermore, the effects of FA addition and water vapour on the conversions of NO in flue gas were investigated [158, 168]. Nevertheless, little research has been done on the effects of water vapour and FA addition on the NOx and SOx gas efficiency improved by pulsed corona discharge [169]. According to experimental research, positive pulsed corona discharge can speed up the conversion of NO and SO_2, and the radicals OH and O, as well as the active species O_3, HO_2, H_2O_2, and others, have a major impact on how well NO and SO_2 is converted. The efficiency of SO_2 conversion is increased by adding water vapour, whereas NO conversion is constrained. The addition of low FA concentration improves the conversion of NO and SO_2 but is significantly reduced by the addition of a high amount of FA. The chemosorption capacity of the FA surface is strengthened by the combined impacts of water vapour and FA addition, which significantly improves the conversion of NO and SO_2. Moreover, the efficacy of NO and SO_2 conversion is considerably influenced by the particular input energy. Under the tested conditions, measured NO and SO_2 conversion efficiencies were roughly 60% and 90%, respectively.

There is evidence that water vapour considerably impacts the elimination of both SO_2 and NO [170]. Under critical circumstances, the adsorption of SO_2 was reduced; however, it was found to increase as the quantity of adsorbed water increased steadily. According to Jozewicz and Rochelle, this behaviour is comparable to that shown for a spray dry flue gas desulphurization method at a temperature of 60–70 °C, where the sorption of SO_2 increased with increasing relative humidity [171]. According to Tsuchiai et al. [170], the reaction processes varied according to the degree to which the H_2O molecules covered the surface of the material. They proposed a theory to explain the occurrence, postulating that SO_2 molecules dissolve in water and combine with $Ca(OH)_2$ to form $Ca(SO_3)\cdot xH_2O$, which then adheres to water layers.

Investigating SO_2's impact on NO removal, Brown et al. [172] proposed that the synthesis of compounds with sulphur and nitrogen is the cause of the high reliance on removing NO in the presence of SO_2. According to Tsuchiai et al. [173], NOx molecules are substituted by SO_2 molecules as calcium consumption of the adsorbent increases. The material was reported to accomplish high calcium utilization at an extended reaction period of 15 h under high concentrations of SO_2, and NO*x* compounds were found to be replaced by SO_2 molecules. As the adsorbed NO is largely substituted for SO_2 throughout the 15 h reaction period, it is advised that the highest NO adsorption be shifted to a lower SO_2 content.

Recently, Zheng et al. [174] examined the removal of NOx using CFA between 50 and 850 °C. The authors reported that at temperatures between 50 and 350 °C, NH_3, NO, and O_2 co-adsorbed on the surface of CFA, and the presence of NO and O_2 inhibited the physical adsorption of NH_3 and encouraged its chemosorption. CFA facilitated NH_3 oxidation by O_2 and NO reduction by NH_3 at 450–850 °C. Oxygen caused the oxidation reaction to predominate and impede the reduction reaction. The FTIR spectra depicting the adsorption of 500 ppm NH_3 and NO after 30 min at varying temperatures are illustrated in Fig. 10. In a study, Wang et al. [175] synthesized manganese oxide-supported FA via a sol–gel method and examined the catalytic oxidation of NO. The outcomes demonstrated that the catalytic efficiency of the catalyst was considerably influenced by the particle size of the catalyst, Mn loading, calcination temperature, and the reaction temperature of NO. It was discovered that 500 °C was the ideal temperature for calcination. The NO catalytic oxidation at a temperature of 290 °C produced the best catalytic oxidation, with a reaction rate of almost 78%, when the FA particle size was between 100 and 200 mesh and the Mn loading was 8 weight percent. According to SEM data, the sol–gel technique produced manganese oxide particles with sizes between 100 and 200 nm that were fairly uniformly loaded on the FA.

A novel CFA supported Gd-Mn-Ti via a sol–gel technique for catalytic conversion of NO by NH_3 [176]. With a large temperature window, the developed 0.2Gd-Mn-Ti/CFA catalyst exhibits above 90% de-NO*x* efficiency from 120 to 330 °C. The causes can be attributed to the fact that adding the optimum amount of Gd can increase acid sites, enhance the redox environment, raise the amount of surface Mn^{4+}, and increase the amount of chemically adsorbable oxygen. Also, the interactions between the Gd-Mn-Ti composite oxides and that between the active ingredients and the carrier contribute to the good reaction activity. Several Mn-Fe-supported FA catalysts were also reported for catalytic reduction of NOx with an efficiency of more than 90% [177]. In a study, Qi et al. [178] fabricated Mn_3O_4-impregnated FA using the impregnation method and studied the removal of NO. The findings demonstrate that catalysts with an Mn concentration of 25 wt% and calcined at a temperature of 400 °C displayed a NO conversion efficiency of more than 80% at 160 °C.

Interaction of NO with FA

Recently, Li et al. [179] reported the removal mechanism of NO using AC/FA-CS adsorbent, as illustrated in Fig. 11. The authors reported that the gaseous NO is initially converted to adsorbed NO over the FA surface through van

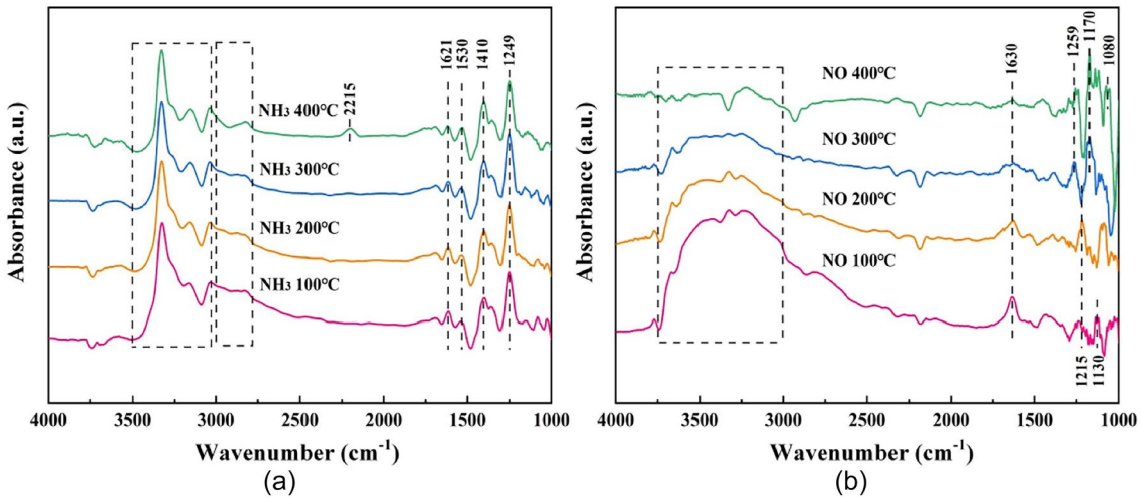

Fig. 10 FTIR spectra after the adsorption of (**a**) NH_3 and (**b**) NO showing the drifts in the IR peaks with varying temperatures (Reproduced with permission from Elsevier) [174]

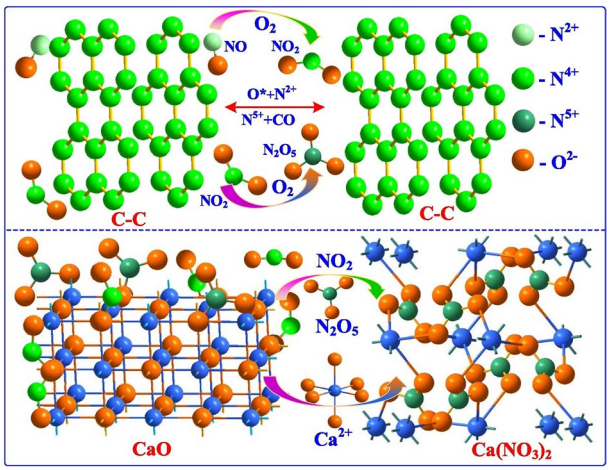

Fig. 11 Mechanism of denitrification process by AC/FA-CS under microwave field (Reproduced with permission from Elsevier) [179]

der Waals interactions. However, the adsorbed NO is unstable and is easily oxidized to NOx by the oxygen-containing functional groups through the energy released by the breakdown of C=C bonds. The carbon media in the adsorbent acts as an active adsorption site for NO*x* and helps capture NO. Secondly, the adsorbed NO is oxidized to NO_2 (N^{+4}) or N_2O_5 (N^{+5}) [180]. The NO_2 is the intermediate product of NO oxidation, which CaO adsorbs in FA-generated $CaNO_3$. The adsorbed N_2O_5 forms $Ca(NO_3)_2$, the major product of the denitrification process. However, the generated $CaNO_3$ and $Ca(NO_3)_2$ could block the adsorbent's active sites, resulting in a decreased adsorption efficiency after a few consecutive adsorption cycles.

Removal of oxides of sulphur

The increasing rates of acid rain could be attributed to the increasing amount of sulphur and nitrogen oxides in the environment emitted by industries, vehicles, and thermal power plants. Furthermore, SO_2 and SO_3 are hazardous gases that lead to the creation of acid particulates that can enter human lungs and get into the bloodstream. Elimination of oxides of sulphur and nitrogen from flue gases is a global threat that needs to be addressed among environmental issues to prevent the pollution of clean air. Flue gases generated from thermal power plants are treated using ammonia-based De-NO*x* and calcium-based De-SO*x* processes. These procedures are reliable and efficient but have high up-front and ongoing expenditures. As a result, there is a growing need for a FGD (flue gas desulphurization) system that is less complicated and more affordable.

Flue gases can be desulphurized using one of three methods: wet, semi-dry, or dry. For the removal of SO_2, the wet-desulphurization process is particularly effective, and gypsum ($CaSO_4{\cdot}2H_2O$) is produced as a useful byproduct. Unfortunately, a significant amount of water is needed, and wastewater treatment is expensive. Semidry procedures are also efficient and use less water compared to wet processes, but it is challenging to implement this process in all circumstances because a significant amount of water is still required to attain a high rate of desulphurization reaction. Due to the need for a lot of water to remove SO_2, wet and semi-dry methods are inappropriate everywhere. Consequently, an affordable dry desulphurization method that requires little water and yields $CaSO_4$ as a useful byproduct is preferred [181]. By reacting SO_2 with solid CaO and creating $CaSO_4$ as a byproduct, Allen and Hayhurst [182] created a

technique to reduce sulphur dioxide emissions, as seen in the following:

$$CaO + SO_2 + 1/2O_2 \rightarrow CaSO_4 \quad (5)$$

Several studies have investigated the adsorption of SO_2 from the air using FA and its composites [183, 184]. Although commercial activated carbon has been widely used for the oxidation of oxides of sulphur, it is prohibitively expensive for large-scale pollutant removal. Numerous researchers have observed that combining FA with $Ca(OH)_2$ or CaO can result in an adsorbent with a higher SO_2 absorption than hydrated lime [185, 186]. As a result, CFA could be used instead of commercial AC as a low-cost adsorbent for dry-type FGD. Because FA is an abundant byproduct of all thermal power plants, using it as a source of silica offers both economic and environmental benefits. The pozzolanic reaction occurs in all situations when FA or silica react with CaO or $Ca(OH)_2$ in a hydration method, forming hydrated calcium silicates. FA treated with Ca(OH)2 has been reported to be a reactive adsorbent for SO_2 removal [187].

To improve desulphurization efficiency, $Ca(OH)_2$/FA materials have been studied for SO_2 adsorption [188, 189]. Matsushima et al. [181] used a circulating fluidized bed with $Ca(OH)_2$/FA sorbent to accomplish a significant SO_2 adsorption without humidifying and the production of primarily $CaSO_4$; 83% SO_2 adsorption efficiency was achieved, the byproducts produced had a high $CaSO_4$ content, and 350 °C was found to be the optimized reaction temperature for desulphurization. Davini et al. [188, 190] also reported desulphurization using a mixture of FA and $Ca(OH)_2$. Their investigation proved that $Ca(OH)_2$/FA mixes were an appealing, low-cost solution for SO_2 reduction. Davini [191] also investigated the adsorption of SO_2 and NOx from flue gases using AC produced from FA. A mixture comparable to commercial AC was reported to have properties similar to commercial AC for removing SOx and NOx from industrial flue gas.

Recently, Li et al. [179, 192] systematically proposed a greater effectiveness and low-cost catalytic sorption method based on the synergetic exploitation of microwave-assisted FA and carbide slag (FA-CS) for desulphurization (De-SOx) and denitrification (De-NO*x*). The mechanism of SO*x* and NO*x* removal is illustrated in Fig. 12. Complete removal of SO_2 from flue gas was achieved within 41 min of treatment. Authors reported that the reversible oxidation and reduction of the coexisting K^{2+}/K^{1+} in the K_2O/FA-CS and K_2O_2/FA-CS catalysts were also beneficial for the catalytic activation that promoted the conversion of S^{4+} to S^{6+}. Moreover, in the K_2O/FA-CS and K_2O_2/FA-CS catalysts, the SO_2 was oxidized to SOx by the active oxygen ($O^{\cdot}$) given by the redox pair K^{2+}/K^{1+}, where the newly created SOx was easily mixed to produce the unstable sulphur complexes in the De-SO_2 process. CFA, CaO, and waste gypsum were used as the raw ingredients in a one-step wet impregnation procedure to create a low-cost and highly activated calcium-based sorbent (ACS) for the removal of SO_2 [193]. With a 100% removal efficiency at 150 °C, the ACS's SO_2 adsorption capacity with CFA/CaO/$CaSO_4$ was high, reaching up to 44.26 mg/g. Furthermore, the production of adsorbed NO_2 or nitrate species with potent oxidizing capabilities might further increase the SO_2 removal efficiency of the ACS in the presence of NO. As a result, the ACS has the advantage of using CFA to remove sulphur dioxide, making it a sustainable sorbent. In a recent study by Qi et al. [194], FA modified with $Ca(OH)_2$ showed increased adsorption of SO_2 compared to FA modified with NaOH in an electrostatic precipitator. The FA/$Ca(OH)_2$ showed an adsorption capacity of 31.44 mg/g, which was almost 142 times higher than that of raw FA.

To establish the influence of the reaction temperature, water vapour pressure, and presence of NO in flue gas, the removal of SO_2 from flue gas by the absorbent made from CFA, CaO, and $CaSO_4$ was researched under various reaction conditions [170]. With a rise in NO content up to 500 ppm at 130 °C, an increase in the SO_2 removal efficiency was observed. When the water vapour pressure rose, the SO_2 adsorption increased until a monolayer of water molecules formed. The SO_2 removal abruptly dropped, and calcium sulphite replaced calcium sulphate as the major product at higher moisture content. With an increasing SO_2 content, the NO adsorption efficiency also increased. Moreover, NO removal increased as the

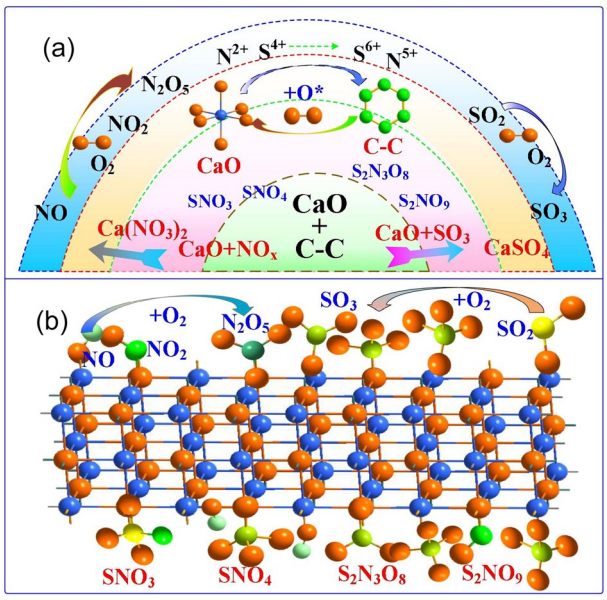

Fig. 12 Simultaneous desulphurization and denitrification mechanism by CFA/CS composite under microwave field (Reproduced with permission from Elsevier) [192]

water vapour pressure rose and significantly decreased when the amount of adsorbed water exceeded the monolayer coverage. The adsorption of oxides of sulphur and nitrogen from flue gas by using sorbents made from $Ca(OH)_2$, $CaSO_4$, silicic acid, and $Al(OH)_3$ was reported by Tsuchiai et al. [195]. As the silica content of the adsorbent grew up to 40%, the adsorption rates of SO_2 and NO also increased. The development of ettringite was only detected by the XRD for the adsorbent having SiO_2 content below 30%, whereas the formation of calcium silicates is indicated to be prevalent in high silica content.

In their study, Lee et al. [196] examined the impact of different variables on the desulphurization activity of adsorbent made from CFA, CaO, and $CaSO_4$ as well as the SSA, reaction temperature, and feed concentrations of NO*x* and SO*x*. It has been noted that while SO_2 concentration fell, the adsorbent desulphurization efficiency increased with increasing SSA, temperature, and NO content. During the flue gas desulphurization process, they [197] also used other types of ash (CFA, bottom ash, oil palm ash, and incinerator ash), and the adsorbent was made by combining the ashes with CaO and $CsSO_4$ using the water hydration method. It has been determined that the best sorbents for absorbing SO_2 are those made from oil palm and CFA. The main byproducts of the hydration reaction are calcium aluminium silicate hydrate compounds, according to an X-ray diffraction spectrum and SEM analysis of the sorbent, which revealed that it was made up of a substance with high structural porosity.

Interaction of SO_2 with FA

The catalytic oxidation and removal mechanism of SO_2 by AC/FA-CS was reported by Li et al. [179], as shown in Fig. 13. Initially, SO_2 is adsorbed on the surface of AC and is then oxidized to SO_3 by adsorbed oxygen on the surface of the adsorbent (Fig. 13a). Then, the CaO in FA adsorbs SO_2 from flue gas, and SO_3 forms the surface of the AC and gets converted into $CaSO_3$. Furthermore, the oxidized SO_3 could also react with CaO, forming $CaSO_4$ (Fig. 13b). Here, the microwave frequency is absorbed by the catalyst to excite S atoms in SO_2 to bind to the AC surface effectively. Microwave energy catalyses the oxidation of SO_2 to SO_3, which could not be achieved under normal conditions [198]. The authors suggested that the enhanced removal of SO_2 could be attributed to the effective oxidation of S^{+4}–S^{+6} by microwave irradiation. Sulphur trioxide has stronger reactivity with the alkaline CaO, and both can react spontaneously to generate $CaSO_4$. However, $CaSO_4$ formed by the reaction of S^{+6} could block the adsorbent's active sites, decreasing the catalyst's removal efficiency.

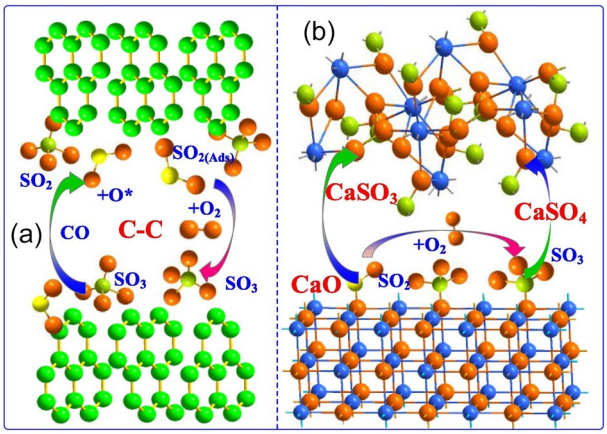

Fig. 13 Mechanism of desulphurization process by AC/FA-CS under microwave field (Reproduced with permission from Elsevier) [179]

Removal of mercury

Due to its devastating effects on both human health and the environment, mercury (Hg), particularly elemental mercury (Hg^0), extracted from thermal power plants, has received much attention. Fly ash is a promising adsorbent that can be used in the method of adsorbent injection to remove Hg^0. Mercury has thus been identified as a potential environmental contaminant. Regulations on mercury emissions from electric utilities have been established by the European Commission and the U.S. EPA, respectively. There are three categories of Hg emission control systems (precombustion, combustion, and flue gas), with the flue gas Hg removal technology being the most used. Mercury that has been oxidized may be removed from the flue gas by current flue gas pollution control systems such as the bag filter, electrostatic precipitator, and wet FGD. Nevertheless, they don't appear to be very effective at removing elemental mercury.

The goal is to convert mercury into oxidized mercury and mercury that is attached to particulates so that it can be successfully removed moving forward. Due to its high removal effectiveness, AC is typically used for removing Hg from flue gas. Because of its high price, AC cannot be used on a wide range [199]. According to studies, the unburned carbon in FA can bind elemental mercury. As a result, FA carbon may be used as a cheap sorbent to remove elemental mercury from gases rather than expensive AC. The unburned carbon removed from FA is a waste product. Any effective use of such substance would be favourable to the entire FA beneficiation process from a financial and ecological standpoint. In order to remove unburned carbon from FA, scientists at Pennsylvania State University have created a procedure that is both efficient and affordable [200]. According to a preliminary investigation, certain unburned fly ash carbon exhibits specific properties for removing Hg^0. These results gave rise

to the idea of using unburned carbon as a cheap sorbent in place of pricey activated carbons to remove Hg^0 from gases, such as utility flue gas. Several factors, including the composition of FA and SSA, the material's morphology, surface pore volume and size volume, and flue gas components, influence the removal of Hg^0 by FA [201].

Numerous studies demonstrate that FA composition is crucial for Hg^0 elimination [202]. Using raw FA, Wang et al. [203] achieved a 60% Hg^0 adsorption efficiency in the flue gas. Compared to the effects of CaO and MgO, adding Al_2O_3, TiO_2, and Fe_2O_3 boosts adsorption efficiency more. Fly ash contains iron species, such as magnetospheres, that facilitate the adsorption of Hg^0, and when the Fe content rises, the ability to remove Hg^0 also rises [202]. Recently, a number of kinetic models were put up to forecast how homogeneous mercury oxidation in flue gas will behave and perform. Nevertheless, occasionally, the catalytic actions of the suspended FA particles prevent these models from doing so correctly. The reaction of Fe_2O_3 contained in FA in the presence of HCl was then identified using a heterogeneous kinetic model. Mercury oxidation efficiency was found to be catalytically active in Fe_2O_3, increasing it to 89.5% at 100 °C.

Fly ash has a relatively low Hg^0 adsorption capacity when compared to AC. Hence, numerous strategies have been investigated to increase fly ash's capacity and stability for Hg^0 removal [204]. Lately, FA modification using Co, Mn and Fe oxides has been used to eliminate elemental mercury from flue gas. According to Xing et al. [205], including Fe and Mn improved the performance of FA adsorbent in the presence of O_2. Due to the oxidation of mercury by enriching well-dispersed Co_3O_4 on the FA surface, co-modified FA created by the wet impregnation method proved successful in Hg^0 removal [206]. Nowadays, commercial halogenated ACs are thought to be the best mercury sorbents available. There are additional financial and environmental benefits to replacing fly ash with AC. Investigations into the capabilities of various fly ash samples treated with $CaCl_2$, $CaBr_2$, and HBr revealed that the mercury removal effectiveness was in the following order: $HBr > CaCl_2 > CaBr_2$ [207]. Mercury species, including $HgCl_2$, HgS, and HgO, are frequently adsorbed by unmodified fly ash, but HgBr-modified fly ash mostly adsorbed $HgBr_2$ and HgO [208].

Song et al. [209] examined the Hg^0 removal behaviour of HBr-modified FA in a fixed-bed reactor and found that it performed noticeably better at removing Hg^0 than unmodified FA. As efficient active sites, the metal and halogen ions in metal halogens enhanced Hg^0 removal efficiency [210]. Due to the presence of Cu^{2+} and Fe^{3+} cations, the loading of $CuBr_2$, $CuCl_2$, and $FeCl_3$ on FA could successfully facilitate the removal of Hg^0 from flue gas [211]. Based on $CuCl_2$-modified FA, a novel magnetic catalyst ($CuCl_2$-MF) was created, and a removal efficiency of 90.6% could be achieved with 6% $CuCl_2$. When HCl was added to the flue gas, the innovative catalyst demonstrated exceptional resistance to SO_2 poisoning [210]. The addition of NO to fly ash that has undergone HBr modification may improve Hg^0 adsorption in an entrained flow reactor. This improvement may be caused by the interaction between HBr and NO when O_2 is present [212]. A good adsorption performance was shown when linked bromide and on-line mechanically modified FA were used to remove mercury at a thermal power station. The coupled bromide and FA showed superior adsorption compared to intrinsic FA and manually modified FA. According to the findings [213], high temperatures were better for Hg^0 removal, and iodine-modified FA performed better at Hg^0 adsorption than bromine- and chlorine-modified FA [214].

Fly ash's ability to adsorb Hg^0 increased by 15 to 25% when an external magnetic force (EMF) was applied, according to He et al. [215]. This rise was brought on by the energy level splitting of mercury brought on by electromagnetic fields (EMF) and the magnetochemistry action of magnetic elements in FA. By virtue of its magnetic properties, FA could also be used to separate sorbents. Fly ash was used to create $(Fe_{2.2}Mn_{0.8})_{1-\delta}O_4$ by Yang et al. [216], who attained an adsorption capacity of > 1.5 mg/g between 100 and 300 °C. The results of treating the magnetic sorbent FeMnOx made from FA with non-thermal plasma showed an increase in Hg0 removal efficiency compared to raw FA [217]. To further improve the effectiveness of its Hg^0 removal, Shi et al. [218] transformed fly ash utilizing non-thermal plasma in the air. The carbonyl and ester groups considerably favoured the Hg0 removal from the sorbent. To remove Hg^0 from simulated flue gas, MnO_2-CeO_2/palygorskite-FA catalysts were created by supporting MnO_2-CeO_2 to palygorskite (PG)-FA [219]. The findings demonstrate that the MnO_2-CeO_2/PG-FA catalyst exhibited outstanding and persistent Hg^0 removal activity, which was mostly attributable to the synergistic effect of MnO_2-CeO_2's catalytic oxidation activity and PG-adsorption FA's capability. At 140 °C, the Mn_8-$Ce_{0.5}$/PG-FA catalyst with a loading of 8.0% MnO_2 and 0.5% CeO_2 demonstrated the best Hg^0 removal efficiency of over 95%. Pyrite (PY) and acid-modified fly ash (AC-FA), which has a stronger Hg^0 removal effect than AC-FA, were combined to create the pyrite-modified fly ash (PY + AC-FA) for mercury removal [220]. About 92% of the mercury removal was achieved at 50 °C with 20 wt% loaded PY/AC-FA. The adsorption process was found to follow a quasi-second-order kinetic model attributed to chemosorption. Furthermore, based on TG-DSC results, it was inferred that Hg^0 is adsorbed on the surface initially and then oxidized to HgS by the FeS_2 present in the pyrite-modified FA. The weight gradually decreased as the temperature rose, reaching 15.2 mg at 420 °C in the end. This suggests that the adsorbed Hg^0 on the surface of

PY + AC-FA starts to evaporate at its boiling point. Xin et al. [221] extracted magnetospheres, modified them with H_2S (S-MS) and employed them for mercury sorption. The selective catalytic oxidation of H_2S resulted in the deposition of elemental sulphur, which has a high affinity for Hg^0, on the surface of the adsorbent. The authors investigated the impact of sulphidation temperature on the adsorption capacity of the adsorbent. The adsorption results revealed 80% removal of Hg^0 in the 50–75 °C temperature range with the S-MS adsorbent treated at a sulphidation temperature of 150 °C for 30 min. The abundance of sulphur species that are capable of binding Hg^0 led to the immobilization of the gaseous Hg^0 by S-MS as stable mercuric sulphide (HgS). The amount of secondary Hg contamination from the industrial waste was reduced because the leaching ratio of Hg from wasted S-MS in wet electrostatic precipitator effluent was almost as low as 1%. The cost analysis reveals that the magnetosphere-based mercury removal technique outperformed commercial AC injection technology in terms of operating costs. As a result, the S-MS showed significant promise for Hg^0 adsorption due to its unique properties, including excellent Hg^0 adsorption capability, reduced environmental hazard, and recyclability.

Few researchers have looked at using zeolites made from FA to remove Hg^0 from flue gas, despite the fact that zeolites have been known to be effective at removing a variety of gaseous pollutants. To create zeolite from fly ashes obtained from coal for the removal of Hg^0, Wang et al. [222] presented a new technique called the supercritical hydrothermal method. The outcomes showed that synthetic zeolites have effective Hg^0 removal capabilities. Ma et al. [223] developed magnetic zeolites from FA using a similar technique to extract Hg^0 from flue gas. The findings demonstrated that the Hg^0 adsorption process followed the Eley–Rideal mechanism, with an efficiency of 92%. Studies have also shown that the presence of magnetic materials in FA can activate the catalytic oxidative capacity, enhancing Hg^0 adsorption. The amount of Hg^0 oxidation increased with the amount of Fe_3O_4 in the FA. In recent research, zeolites fabricated using class F and class C fly ash and modified with Fe and Ag nanoparticles were employed for the removal of elemental mercury from the flue gas [224]. The schematic illustration of a simultaneous zeolite synthesis and modification process is shown in Fig. 14. Compared to Fe-modified zeolite, Ag-modified zeolite showed excellent performance and stability up to 350 °C towards the removal of Hg^0 from flue gas.

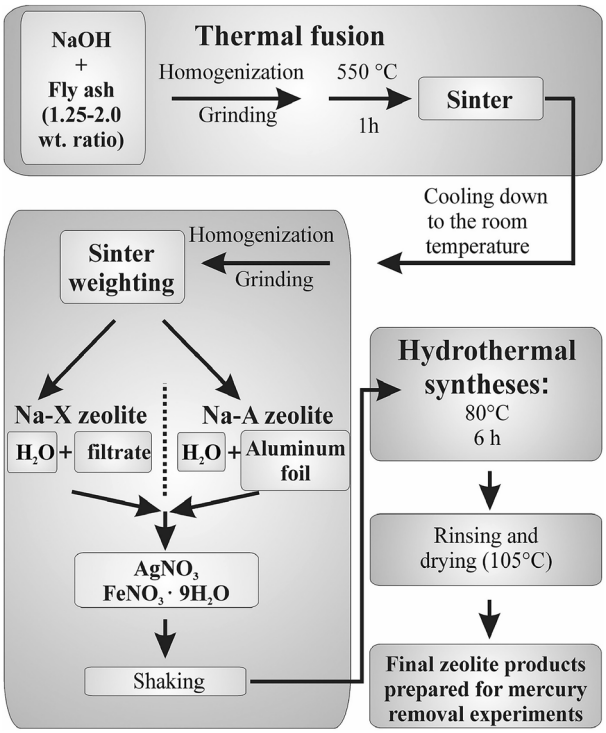

Fig. 14 A schematic diagram of zeolite's simultaneous synthesis and modification process (Reproduced with permission from Elsevier) [224]

Interaction of Hg with FA

Research has shown that several FAs are affixed to mercury and its compounds in the flue gases. The removal of mercury is based on its oxidation to HgO or $HgCl_2$ by different functional groups on fly ash surfaces. Several inorganic species like SO_2 and Fe_2O_3, which oxidize mercury, favour its removal. However, the adsorption interaction of Hg with FA is still not validated, and some variables need to be explored. Zhu et al. [225] investigated mercury adsorption onto different types of modified fly ash and reported the interaction mechanism of Hg with FA. FA modified with $FeCl_3$ reacted with elemental mercury to form HgCl and $HgCl_2$, removing mercury from flue gas. The laboratory-based experiments showed that the presence of unburned carbon in the FA plays a major role in retaining mercury on the surface of the FA.

Furthermore, the role of unburned carbon and its structure (anisotropic, fused, porous) on mercury uptake must also be investigated. FA could be a potential material for the removal of different compounds of Hg depending on the nature of mercury compounds, but the variation in the removal efficiency could be due to the anisotropic nature of the unburned carbon. The physiochemical interactions between carbon and mercury may be responsible for mercury adsorption on FA. The oxygen-containing functional groups [OH/C–O, C=O, C(O)–O–C, and (O–C=O)–O] present due to the unburned carbon oxidize elemental mercury and result in the adsorption of mercury over the FA surface. The active sites on the unburned carbon acted as primary adsorption centres having a high affinity for mercury compounds, which further act as primary sites for multilayer mercury adsorption [226]. The adsorption isotherms and

the characterization techniques revealed that the adsorption of Hg is higher at those sites containing oxygen-containing functional groups. Oxidized activated carbon at 400 °C showed a higher affinity for mercury compounds compared to pure activated carbon, signifying that oxygen-containing functional groups are essential for mercury adsorption [201].

Conclusion

This review has summarized the research on the preparation, characterization, and photodegradation of organic compounds and the adsorption of toxic gases utilizing fly ash. FA-based photocatalysts are a new sector of FA usage, and a new era of photodegradation of organic molecules has emerged as a possible method for wastewater treatment. Due to its high SSA, adequate pore size, high porosity, high CaO content, and surface functional groups, FA can be employed as the basis material of various adsorbents to treat air and water pollutants. FA contains unburned carbon, which is essential for removing various air pollutants. The sorption capacity can be increased by turning the unburned carbon into AC. Fly ash nanocomposites are very effective at adsorbing pollutants from the air and water, including heavy metals, poisonous organic dyes, VOCs, SO*x*, and NO*x*. This review discussed the mechanism of the photocatalytic degradation of dyes and the applicability of FA for removing toxic pollutants from the flue gas. As a result, efforts should be made to establish procedures to use CFA for environmental remediation effectively.

Future prospects

The development of FA-based photocatalysts has revolutionized the use of FA for water remediation. More research is needed, however, to improve the photodegradation effectiveness of FA-based photocatalysts. Doping can be used to solve the problem of a greater bandgap, but the proper dopant must be chosen. Although TiO_2 is the most commonly studied photocatalyst, there are still several additional photocatalysts that, when utilized for dye photodegradation, can make a significant difference in the rate of photocatalytic degradation.

Most of the researchers focused on the degradation of dyes by using fly ash-based photocatalysts. Still, very little research is available on the photocatalytic degradation of other organic contaminants. Photocatalytic degradation of other emerging organic contaminants, such as phenols, pesticides, persistent organic pollutants (POP), and pharmaceutical compounds using fly ash-based photocatalyst systems, can be an interesting topic for further studies. In a multi-pollutant system, hazardous pollutants cannot be removed due to TiO_2's extremely selective character. More studies are needed in order to alter TiO_2-FACs to adsorb and degrade numerous different pollutants in a multi-pollutant system.

There are scarce data available on the percentage loading of photocatalyst nanoparticles on fly ash support. Therefore, budding researchers should pay more attention to this area of research in the near future. Also, no pilot study is available on the use of fly ash photocatalysts for real industrial wastewater. However, Ashour et al. [166] successfully adsorbed 100% copper, zinc, and iron from industrial wastewater, maintaining a flow rate of 200 L/h. Therefore, fly ash photocatalysts should also be examined on a pilot scale.

The highly effective adsorption and catalytic oxidation of mercury have been reported on carbon-, metal-, and natural mineral-based composites. The unsolved issues with Hg removal include the following: (i) how to improve the anti-poisoning properties of Hg^0 catalysts against co-existing gases like SO_2 and NH_3; (ii) how to create innovations that effectively prevent the elimination of toxic components produced during the removal process; (iii) how to establish interaction mechanisms for Hg^0 oxidation in homogeneous and heterogeneous reactions. In addition, it is recommended that particulate matter, NO*x*, and SO_2 be simultaneously removed in order to control mercury emission. So, there should be further research into investigating economical mercury removal technologies. Further research should thoroughly assess these materials' biocompatibility, environmental protection, and ecotoxicology.

FA modification and the creation of fly ash-based molecular sieves may become more difficult and expensive at the same time, which could pose a problem for large-scale applications. Maintaining a good balance between cost control and performance enhancement is important. The main issues that need to be resolved in the future are the creation of less expensive modification techniques and easier molecular sieve production procedures. To modify and create new fly ash-based adsorbents with more highly active sites and developed porous structures, some current efficient green advanced oxidation technologies and new methods for synthesizing porous materials are suggested.

We are all aware that the presence of SO*x*/NO*x*/CO_2/H_2S/CO/VOCs pollutants in flue gas has a detrimental impact on the efficiency and stability of the adsorbents, which raises the cost of operation. Hence, creating fly ashes-based, more resistant adsorbents would be advantageous. Cerium and lanthanum are two rare earth elements that cannot be corroded easily. Studying the composite adsorbent of FA and these rare earth metal components is thus needed. Several transition metal oxide combinations have also been shown to be effective corrosion resistance for creating more stable fly ash-based adsorbents.

Lastly, the adsorption mechanism of SO*x*, NO*x* and mercury compounds on the FA still needs to be explored

to understand these pollutants' interactions with the adsorbent. Understanding the interaction mechanism will help the new scientists develop new and modified adsorbents based on FA with enhanced adsorption capacity to remove these pollutants effectively and selectively.

Data availability All of the materials investigated during the study are included in this published article, along with the data that supported the findings.

Declarations

Conflict of interest On behalf of all authors, the corresponding author states that there is no conflict of interest.

References

1. Gadore V, Ahmaruzzaman M (2021) Tailored fly ash materials: a recent progress of their properties and applications for remediation of organic and inorganic contaminants from water. J Water Process Eng. https://doi.org/10.1016/j.jwpe.2020.101910
2. An C, Yang S, Huang G et al (2016) Removal of sulfonated humic acid from aqueous phase by modified coal fly ash waste: equilibrium and kinetic adsorption studies. Fuel 165:264–271. https://doi.org/10.1016/J.FUEL.2015.10.069
3. Aigbe UO, Ukhurebor KE, Onyancha RB et al (2021) Fly ash-based adsorbent for adsorption of heavy metals and dyes from aqueous solution: a review. J Mater Res Technol 14:2751–2774. https://doi.org/10.1016/J.JMRT.2021.07.140
4. Mishra SR, Gadore V, Verma R et al (2023) In2S3 incorporated into CO32−@Ni/Fe/Zn trimetallic LDH as a bi-functional novel nanomaterial for enzymatic urea sensing and removal of sulfur-containing pharmaceutical from aqueous streams. Chem Eng J. https://doi.org/10.1016/J.CEJ.2023.146207
5. Ahmaruzzaman M, Mishra SR (2021) Photocatalytic performance of g-C3N4 based nanocomposites for effective degradation/removal of dyes from water and wastewater. Mater Res Bull 143:111417. https://doi.org/10.1016/J.MATERRESBULL.2021.111417
6. Mishra SR, Ahmaruzzaman M (2022) Tin oxide based nanostructured materials: synthesis and potential applications. Nanoscale 14:1566–1605. https://doi.org/10.1039/D1NR07040A
7. Mishra SR, Ahmaruzzaman M (2021) Cerium oxide and its nanocomposites: structure, synthesis, and wastewater treatment applications. Mater Today Commun 28:102562. https://doi.org/10.1016/J.MTCOMM.2021.102562
8. Anastopoulos I, Pashalidis I, Orfanos AG et al (2020) Removal of caffeine, nicotine and amoxicillin from (waste)waters by various adsorbents: a review. J Environ Manage 261:110236. https://doi.org/10.1016/J.JENVMAN.2020.110236
9. Kumar V, Saharan P, Sharma AK et al (2020) Silver doped manganese oxide-carbon nanotube nanocomposite for enhanced dye-sequestration: Isotherm studies and RSM modelling approach. Ceram Int 46:10309–10319. https://doi.org/10.1016/J.CERAMINT.2020.01.025
10. Tong Y, Gao J, Yue T et al (2023) Distribution, chemical fractionation, and potential environmental risks of Hg, Cr, Cd, Pb, and As in wastes from ultra-low emission coal-fired industrial boilers in China. J Hazard Mater 446:130606. https://doi.org/10.1016/J.JHAZMAT.2022.130606
11. Bhattacharyya A, Kerketta S, Kumar MS, Rajanikanth BS (2014) Discharge plasma cascaded with fly ash for removal of NOx in biodiesel exhaust: a feasibility study. Int J Plasma Environ Sci Technol 8:98–102
12. Izquierdo MT, Rubio B (2008) Carbon-enriched coal fly ash as a precursor of activated carbons for SO2 removal. J Hazard Mater 155:199–205. https://doi.org/10.1016/J.JHAZMAT.2007.11.047
13. Boycheva S, Szegedi Á, Lázár K et al (2023) Advanced high-iron coal fly ash zeolites for low-carbon emission catalytic combustion of VOCs. Catal Today 418:114109. https://doi.org/10.1016/J.CATTOD.2023.114109
14. Mohan D, Singh KP, Singh G, Kumar K (2002) Removal of dyes from wastewater using flyash, a low-cost adsorbent. Ind Eng Chem Res 41:3688–3695. https://doi.org/10.1021/IE010667
15. Agarwal S, Rani A (2017) Adsorption of resorcinol from aqueous solution onto CTAB/NaOH/flyash composites: equilibrium, kinetics and thermodynamics. J Environ Chem Eng 5:526–538. https://doi.org/10.1016/J.JECE.2016.11.035
16. Chinh NT, Mai TT, Thi N et al (2017) Using fly ash treated by NaOH and H2SO4 solutions for Hg2+ and Cd2+ ion adsorption. Vietnam J Chem 55:196. https://doi.org/10.15625/2525-2321.2017-00443
17. Xiyili H, Çetintaş S, Bingöl D (2017) Removal of some heavy metals onto mechanically activated fly ash: modeling approach for optimization, isotherms, kinetics and thermodynamics. Process Saf Environ Prot 109:288–300. https://doi.org/10.1016/J.PSEP.2017.04.012
18. Drunka R, Grabis J, Krumina A (2016) Microwave assisted synthesis, modification with platinum and photocatalytical properties of TiO2 nanofibers. Medziagotyra 22:138–141. https://doi.org/10.5755/J01.MS.22.1.7353
19. Yadav HM, Kim JS (2016) Pawar SH (2016) Developments in photocatalytic antibacterial activity of nano TiO2: a review. Korean J Chem Eng 337(33):1989–1998. https://doi.org/10.1007/S11814-016-0118-2
20. Lv J, Sheng T, Su L et al (2013) N, S co-doped-TiO2/fly ash beads composite material and visible light photocatalytic activity. Appl Surf Sci 284:229–234. https://doi.org/10.1016/J.APSUSC.2013.07.086
21. Udom I, Ram MK, Stefanakos EK et al (2013) One dimensional-ZnO nanostructures: synthesis, properties and environmental applications. Mater Sci Semicond Process 16:2070–2083. https://doi.org/10.1016/J.MSSP.2013.06.017
22. Zhang J, Cui H, Wang B et al (2013) Fly ash cenospheres supported visible-light-driven BiVO4 photocatalyst: synthesis, characterization and photocatalytic application. Chem Eng J 223:737–746. https://doi.org/10.1016/J.CEJ.2012.12.065
23. Zhang J (2014) Preparation of Novel Pt–BiVO4/Fly ash cenospheres composites with high photocatalytic performance. Adv Mater Res 1010–1012:216–219. https://doi.org/10.4028/WWW.SCIENTIFIC.NET/AMR.1010-1012.216
24. Gadore V, Mishra SR, Ahmaruzzaman M (2024) Bandgap engineering approach for synthesising photoactive novel Ag/HAp/SnS2 for removing toxic anti-fungal pharmaceutical from aqueous environment. J Hazard Mater 461:132458. https://doi.org/10.1016/J.JHAZMAT.2023.132458
25. Mishra SR, Gadore V, Ahmaruzzaman M (2023) Insights into persulfate-activated photodegradation of tinidazole and photoreduction of hexavalent chromium through β-In2S3 anchored on Ag-doped fish scale-derived HAp composite quantum dots. J Clean Prod. https://doi.org/10.1016/J.JCLEPRO.2023.139221
26. Mosleh S, Rahimi MR, Ghaedi M et al (2018) Sonochemical-assisted synthesis of CuO/Cu2O/Cu nanoparticles as efficient photocatalyst for simultaneous degradation of pollutant dyes in rotating packed bed reactor: LED illumination and central

composite design optimization. Ultrason Sonochem 40:601–610. https://doi.org/10.1016/J.ULTSONCH.2017.08.007
27. Hassan SA, El-Salamony RA (2014) Photocatalytic disc-shaped composite systems for removal of hazardous dyes in aqueous solutions establish a green direct routes for propylene epoxidation using multi-component molybdenum oxide catalysts view project catalytic study view project photocatalytic disc-shaped composite systems for removal of hazardous dyes in aqueous solutions. 2:1–56. https://doi.org/10.13179/canchemtrans.2014.02.01.0057
28. Ahmaruzzaman M, Gadore V (2021) MoS2 based nanocomposites: an excellent material for energy and environmental applications. J Environ Chem Eng 9:105836. https://doi.org/10.1016/J.JECE.2021.105836
29. Lum PT, Foo KY, Zakaria NA, Palaniandy P (2020) Ash based nanocomposites for photocatalytic degradation of textile dye pollutants: a review. Mater Chem Phys 241:122405. https://doi.org/10.1016/J.MATCHEMPHYS.2019.122405
30. Son BT, Long NV, Nhat Hang NT (2021) Fly ash-, foundry sand-, clay-, and pumice-based metal oxide nanocomposites as green photocatalysts. RSC Adv 11:30805–30826. https://doi.org/10.1039/D1RA05647F
31. Chuaicham C, Inoue T, Balakumar V et al (2022) Visible light-driven ZnCr double layer oxide photocatalyst composites with fly ashes for the degradation of ciprofloxacin. J Environ Chem Eng 10:106970. https://doi.org/10.1016/J.JECE.2021.106970
32. Nadeem N, Zahid M, Rehan ZA et al (2022) Improved photocatalytic degradation of dye using coal fly ash-based zinc ferrite (CFA/ZnFe2O4) composite. Int J Environ Sci Technol 19:3045–3060. https://doi.org/10.1007/S13762-021-03255-9/TABLES/2
33. Nadeem N, Yaseen M, Rehan ZA et al (2022) Coal fly ash supported CoFe2O4 nanocomposites: synergetic Fenton-like and photocatalytic degradation of methylene blue. Environ Res 206:112280. https://doi.org/10.1016/J.ENVRES.2021.112280
34. Barman S, Chakraborty R (2021) Sustainable HMF synthesis from waste cooked rice water using fly-ash based Al2SiO5 supported nano-photocatalyst under halogen-ultrasound synergistic-energy: LCA and DFT based simulation. J Environ Chem Eng 9:106736. https://doi.org/10.1016/J.JECE.2021.106736
35. Ishag A, Yue Y, Xiao J et al (2022) Recent advances on the adsorption and oxidation of mercury from coal-fired flue gas: a review. J Clean Prod 367:133111. https://doi.org/10.1016/J.JCLEPRO.2022.133111
36. Vega-Mendoza MS, Luévano-Hipólito E, Torres-Martínez LM (2021) Design and fabrication of photocatalytic coatings with α/β-Bi2O3 and recycled-fly ash for environmental remediation and solar fuel generation. Ceram Int 47:26907–26918. https://doi.org/10.1016/J.CERAMINT.2021.06.100
37. Ökte AN, Karamanis D (2013) A novel photoresponsive ZnO-flyash nanocomposite for environmental and energy applications. Appl Catal B Environ 142–143:538–552. https://doi.org/10.1016/J.APCATB.2013.05.045
38. Kim HJ, Joshi MK, Pant HR et al (2015) One-pot hydrothermal synthesis of multifunctional Ag/ZnO/fly ash nanocomposite. Colloids Surfaces A Physicochem Eng Asp 469:256–262. https://doi.org/10.1016/J.COLSURFA.2015.01.032
39. Fraga TJM, de Araújo CMB, da Motta Sobrinho MA, Ghislandi MG (2021) The role of multifunctional nanomaterials in the remediation of textile wastewaters. Sustain Technol Text Wastewater Treat. https://doi.org/10.1016/B978-0-323-85829-8.00001-8
40. Adair JH, Suvaci E (2001) Submicron electroceramic powders by hydrothermal synthesis. Encycl Mater Sci Technol. https://doi.org/10.1016/B0-08-043152-6/01607-7
41. Mushtaq F, Zahid M, Mansha A et al (2020) MnFe2O4/coal fly ash nanocomposite: a novel sunlight-active magnetic photocatalyst for dye degradation. Int J Environ Sci Technol 17:4233–4248. https://doi.org/10.1007/S13762-020-02777-Y/FIGURES/10
42. Favier L, Harja M (2020) TiO2/Fly ash nanocomposite for photodegradation of organic pollutant. Handb Nanomater Nanocomposites Energy Environ Appl. https://doi.org/10.1007/978-3-030-11155-7_11-2
43. Wang B, Yang Z, An H et al (2015) Photocatalytic activity of Pt–TiO2 films supported on hydroxylated fly ash cenospheres under visible light. Appl Surf Sci 324:817–824. https://doi.org/10.1016/J.APSUSC.2014.11.046
44. Oleszczuk P, Pan B, Xing B (2009) Adsorption and desorption of oxytetracycline and carbamazepine by multiwalled carbon nanotubes. Environ Sci Technol 43:9167–9173. https://doi.org/10.1021/ES901928Q/SUPPL_FILE/ES901928Q_SI_001.PDF
45. Zhang X, Cresswell M (2015) Inorganic controlled release technology: materials and concepts for advanced drug formulation. Butterworth-Heinemann
46. Kemnitz E, Noack J (2015) The non-aqueous fluorolytic sol–gel synthesis of nanoscaled metal fluorides. Dalt Trans 44:19411–19431. https://doi.org/10.1039/C5DT00914F
47. Rao BG, Mukherjee D, Reddy BM (2017) Novel approaches for preparation of nanoparticles. Nanostruct Nov Ther Synth Charact Appl. https://doi.org/10.1016/B978-0-323-46142-9.00001-3
48. Wang B, Li Q, Wang W et al (2011) Preparation and characterization of Fe3+-doped TiO2 on fly ash cenospheres for photocatalytic application. Appl Surf Sci 257:3473–3479. https://doi.org/10.1016/J.APSUSC.2010.11.050
49. Li G, Teng Q, Sun B et al (2021) Synthesis scaly Ag-TiO2 loaded fly ash magnetic bead particles for treatment of xanthate wastewater. Colloids Surfaces A Physicochem Eng Asp 624:126795. https://doi.org/10.1016/J.COLSURFA.2021.126795
50. Chuaicham C, Inoue T, Balakumar V et al (2022) Fabrication of visible-light-active ZnCr mixed metal oxide/fly ash for photocatalytic activity toward pharmaceutical waste ciprofloxacin. J Ind Eng Chem 108:263–273. https://doi.org/10.1016/J.JIEC.2022.01.006
51. Hadisantoso EP, Ayu ZD, Listiani P, Setiadji S (2021) Synthesis of ZnO/FA composite for methylene blue decolorization. IOP Conf Ser Mater Sci Eng 1098:062066. https://doi.org/10.1088/1757-899X/1098/6/062066
52. Luévano-Hipólito E, Torres-Martínez LM, Cantú-Castro LVF (2019) Self-cleaning coatings based on fly ash and bismuth-photocatalysts: Bi2O3, Bi2O2CO3, BiOI, BiVO4, BiPO4. Constr Build Mater 220:206–213. https://doi.org/10.1016/J.CONBUILDMAT.2019.06.030
53. Shaban M, Abukhadra MR, Hamd A et al (2017) Photocatalytic removal of Congo red dye using MCM-48/Ni2O3 composite synthesized based on silica gel extracted from rice husk ash; fabrication and application. J Environ Manage 204:189–199. https://doi.org/10.1016/J.JENVMAN.2017.08.048
54. An N, Ma Y, Liu J et al (2018) Enhanced visible-light photocatalytic oxidation capability of carbon-doped TiO2 via coupling with fly ash. Chin J Catal 39:1890–1900. https://doi.org/10.1016/S1872-2067(18)63152-3
55. Ramakrishna S, Fujihara K, Teo WE et al (2006) Electrospun nanofibers: solving global issues. Mater Today 9:40–50. https://doi.org/10.1016/S1369-7021(06)71389-X
56. Saud PS, Pant B, Park M et al (2015) Preparation and photocatalytic activity of fly ash incorporated TiO2 nanofibers for effective removal of organic pollutants. Ceram Int 41:1771–1777. https://doi.org/10.1016/J.CERAMINT.2014.09.123
57. Leontie L, Caraman M, Alexe M, Harnagea C (2002) Structural and optical characteristics of bismuth oxide thin films. Surf Sci 507–510:480–485. https://doi.org/10.1016/S0039-6028(02)01289-X

58. Weidong H, Wei Q, Xiaohong W et al (2007) The photocatalytic properties of bismuth oxide films prepared through the sol–gel method. Thin Solid Films 515:5362–5365. https://doi.org/10.1016/J.TSF.2007.01.031
59. Cui X, Shi J, Ye Z et al (2014) Layer-by-layer assembly and photocatalytic activity of titania nanosheets on coal fly ash microspheres. Int J Photoenergy. https://doi.org/10.1155/2014/823078
60. Sietsma JRA, Jos van Dillen A, de Jongh PE, de Jong KP (2006) Application of ordered mesoporous materials as model supports to study catalyst preparation by impregnation and drying. Stud Surf Sci Catal 162:95–102. https://doi.org/10.1016/S0167-2991(06)80895-5
61. Adam F, Appaturi JN, Thankappan R, Nawi MAM (2010) Silica–tin nanotubes prepared from rice husk ash by sol–gel method: characterization and its photocatalytic activity. Appl Surf Sci 257:811–816. https://doi.org/10.1016/J.APSUSC.2010.07.070
62. Xu Y, Hu E, Xu D, Guo Q (2021) Activation of peroxymonosulfate by bimetallic CoMn oxides loaded on coal fly ash-derived SBA-15 for efficient degradation of Rhodamine B. Sep Purif Technol 274:119081. https://doi.org/10.1016/J.SEPPUR.2021.119081
63. Yadav G, Yadav N, Gadore V et al (2023) Biogenic growth of egg shell–derived CaMn2O4 over tailored FLY ASH surface for synergistically photodegradation of ofloxacin: materialistic and chemical studies. Biomass Convers Biorefinery 1:1–18. https://doi.org/10.1007/S13399-023-04978-0/FIGURES/19
64. Lin L, Huang M, Long L, Chen D (2014) Novel photocatalysts of fly ash cenospheres supported BiOBr hierarchical microspheres with high photocatalytic performance. J Alloys Compd 615:929–932. https://doi.org/10.1016/J.JALLCOM.2014.06.088
65. Ahmed AE, Adam F (2007) Indium incorporated silica from rice husk and its catalytic activity. Microporous Mesoporous Mater 103:284–295. https://doi.org/10.1016/J.MICROMESO.2007.01.055
66. Coronado JM, Fresno F, Hernández-Alonso MD, Portela R (2013) Design of advanced photocatalytic materials for energy and environmental applications. Springer
67. Coronado JM (2013) A historical introduction to photocatalysis. Green Energy Technol 71:1–4. https://doi.org/10.1007/978-1-4471-5061-9_1/FIGURES/1
68. Adam F, Appaturi JN, Khanam Z et al (2013) Utilization of tin and titanium incorporated rice husk silica nanocomposite as photocatalyst and adsorbent for the removal of methylene blue in aqueous medium. Appl Surf Sci 264:718–726. https://doi.org/10.1016/J.APSUSC.2012.10.106
69. Chekuri RD, Tirukkovalluri SR (2017) Synthesis of cobalt doped titania nano material assisted by gemini surfactant: characterization and application in degradation of Acid Red under visible light irradiation. South Afr J Chem Eng 24:183–195. https://doi.org/10.1016/J.SAJCE.2017.10.001
70. Kabir MH, Kabir MF, Nigar F et al (2012) Preparation and characterization of rice husk ash (RHA)-TiO2/ZnO composites and its application in treating effluents from textile industries. Bangladesh J Sci Ind Res 47:445–448. https://doi.org/10.3329/BJSIR.V47I4.14075
71. Schrauzer GN (2011) Photoreduction of nitrogen on TiO2 and TiO2-containing minerals. Green Energy Technol 33:601–623. https://doi.org/10.1007/978-0-85729-638-2_18/TABLES/4
72. Vinu R, Madras G (2011) Photocatalytic degradation of water pollutants using nano-TiO2. Green Energy Technol 33:625–677. https://doi.org/10.1007/978-0-85729-638-2_19/TABLES/8
73. Xu N, Shi Z, Fan Y et al (1999) Effects of particle size of TiO2 on photocatalytic degradation of methylene blue in aqueous suspensions. Ind Eng Chem Res 38:373–379. https://doi.org/10.1021/IE980378U/ASSET/IMAGES/LARGE/IE980378UF00011.JPEG
74. Borges ME, Alvarez-Galván MC, Esparza P et al (2008) Ti-containing volcanic ash as photocatalyst for degradation of phenol. Energy Environ Sci 1:364–369. https://doi.org/10.1039/B802187M
75. Naiya TK, Bhattacharya AK, Mandal S, Das SK (2009) The sorption of lead(II) ions on rice husk ash. J Hazard Mater 163:1254–1264. https://doi.org/10.1016/J.JHAZMAT.2008.07.119
76. Chandrasekhar S, Pramada PN, Praveen L (2005) Effect of organic acid treatment on the properties of rice husk silica. J Mater Sci 40:6535–6544. https://doi.org/10.1007/S10853-005-1816-Z/METRICS
77. An D, Guo Y, Zou B et al (2011) A study on the consecutive preparation of silica powders and active carbon from rice husk ash. Biomass Bioenerg 35:1227–1234. https://doi.org/10.1016/J.BIOMBIOE.2010.12.014
78. Lataye DH, Mishra IM, Mall ID (2008) Pyridine sorption from aqueous solution by rice husk ash (RHA) and granular activated carbon (GAC): parametric, kinetic, equilibrium and thermodynamic aspects. J Hazard Mater 154:858–870. https://doi.org/10.1016/J.JHAZMAT.2007.10.111
79. Fatimah I, Said A, Hasanah UA (2015) Preparation of TiO2-SiO2 using rice husk ash as silica source and the kinetics study as photocatalyst in methyl violet decolorization. Bull Chem React Eng Catal 10:43–49. https://doi.org/10.9767/BCREC.10.1.7218.43-49
80. Wang S (2008) Application of solid ash based catalysts in heterogeneous catalysis. Environ Sci Technol 42:7055–7063. https://doi.org/10.1021/ES801312M/SUPPL_FILE/ES801312M_SI_001.PDF
81. Kim HJ, Kim CS (2014) Synthesis and characterization of zno/fly ash composite with highly photocatalytic activity using a hydrothermal process. Dig J Nanomater Biostruct 9:997–1006
82. Esparza P, Borges ME, Díaz L et al (2010) Photodegradation of dye pollutants using new nanostructured titania supported on volcanic ashes. Appl Catal A Gen 388:7–14. https://doi.org/10.1016/J.APCATA.2010.07.058
83. Wahyuni ET, Suherman S, Setyawati D et al (2020) Photocatalytic activity of TiO2/SiO2 prepared from silica contained in volcanic ash for ammonia removaL. Rasayan J Chem 13:574–584. https://doi.org/10.31788/RJC.2020.1315464
84. Wei TY, Kuo CY, Hsu YJ et al (2008) Tin oxide nanocrystals embedded in silica aerogel: photoluminescence and photocatalysis. Microporous Mesoporous Mater 112:580–588. https://doi.org/10.1016/J.MICROMESO.2007.10.040
85. Malwal D, Gopinath P (2016) Enhanced photocatalytic activity of hierarchical three dimensional metal oxide@CuO nanostructures towards the degradation of Congo red dye under solar radiation. Catal Sci Technol 6:4458–4472. https://doi.org/10.1039/C6CY00128A
86. Chatti R, Rayalu SS, Dubey N et al (2007) Solar-based photoreduction of methyl orange using zeolite supported photocatalytic materials. Sol Energy Mater Sol Cells 91:180–190. https://doi.org/10.1016/J.SOLMAT.2006.08.009
87. Nourmoradi H, Zabihollahi S, Pourzamani HR (2015) Removal of a common textile dye, navy blue (NB), from aqueous solutions by combined process of coagulation–flocculation followed by adsorption. New pub Balaban 57:5200–5211. https://doi.org/10.1080/19443994.2014.1003102
88. Gupta VK, Nayak A, Agarwal S (2015) Bioadsorbents for remediation of heavy metals: current status and their future prospects. Environ Eng Res 20:1–18. https://doi.org/10.4491/eer.2015.018
89. Yadav G, Mishra SR, Gadore V et al (2023) A smart and sustainable pathway for abatement of single and binary mixtures of dyes through magnetically retrievable Ca4Fe9O17 anchored on Biochar matrix. Sci Rep 13:1–21. https://doi.org/10.1038/s41598-023-40077-w

90. Manganelli S, Benfenati E, Manganaro A et al (2016) New quantitative structure-activity relationship models improve predictability of ames mutagenicity for aromatic AZO compounds. Toxicol Sci 153:316–326. https://doi.org/10.1093/TOXSCI/KFW125
91. Gadore V, Mishra SR, Ahmaruzzaman M (2023) Facile green synthesis of SnS2 nanoparticles using Tulsi extract: insight into the optical and photocatalytic properties. Int J Environ Anal Chem. https://doi.org/10.1080/03067319.2023.2178912/SUPPL_FILE/GEAC_A_2178912_SM0330.PDF
92. Mohammadi N, Khani H, Gupta VK et al (2011) Adsorption process of methyl orange dye onto mesoporous carbon material–kinetic and thermodynamic studies. J Colloid Interface Sci 362:457–462. https://doi.org/10.1016/J.JCIS.2011.06.067
93. Mishra SR, Gadore V, Ahmaruzzaman M (2023) Novel 3D sphere-like β-In2S3/Biochar nanoflowers for remediation of dyes in single and binary systems and interpretation using statistical physical modeling. Environ Nanotechnol Monit Manag 20:100807. https://doi.org/10.1016/j.enmm.2023.100807
94. Ameta N, Sharma J, Sharma S et al (2012) Copper modified iron oxide as heterogeneous photo-Fenton reagent for the degradation of coomasie brilliant blue R-250. Indian J Chem -Section A 51:943–948
95. Subramanian E (2015) Development of iron oxide/zeo-nax nano photocatalyst from coal fly ash and its activity assessment by methylene blue dye degradation organic and Inorganic hybrid materials for photocatalytic applications view project utilization of waste materials view pr. Int Res J Nat Appl Sci 2:114–128
96. Ren C, Yang B, Wu M et al (2010) Synthesis of Ag/ZnO nanorods array with enhanced photocatalytic performance. J Hazard Mater 182:123–129. https://doi.org/10.1016/J.JHAZMAT.2010.05.141
97. Dey AK, Mishra SR, Ahmaruzzaman M (2023) Solar light–based advanced oxidation processes for degradation of methylene blue dye using novel Zn-modified CeO2@biochar. Environ Sci Pollut Res 30:53887–53903. https://doi.org/10.1007/S11356-023-26183-2/TABLES/1
98. Li C, Wang B, Cui H et al (2013) Preparation and characterization of buoyant nitrogen-doped TiO2 composites supported by fly ash cenospheres for photocatalytic applications. J Mater Sci Technol 29:835–840. https://doi.org/10.1016/J.JMST.2013.04.027
99. Zhu J, Liu S, Ge J et al (2016) Synthesis of Fe2O3-TiO2/fly-ash-cenosphere composite and its mechanism of photocatalytic oxidation under visible light. Res Chem Intermed 42:3637–3654. https://doi.org/10.1007/S11164-015-2236-6/FIGURES/13
100. Huo P, Yan Y, Li S et al (2010) H2O2 modified surface of TiO2/fly-ash cenospheres and enhanced photocatalytic activity on methylene blue. Desalination 263:258–263. https://doi.org/10.1016/J.DESAL.2010.06.067
101. Kalpana K, Selvaraj V (2015) Photodegradation and antibacterial studies of ZnS enwrapped fly ash nanocomposite for multipurpose industrial applications. RSC Adv 5:47766–47777. https://doi.org/10.1039/C4RA16642F
102. El Qada EN, Allen SJ, Walker GM (2006) Adsorption of Methylene Blue onto activated carbon produced from steam activated bituminous coal: a study of equilibrium adsorption isotherm. Chem Eng J 124:103–110. https://doi.org/10.1016/J.CEJ.2006.08.015
103. Zhang Y, Liu L (2013) Fly ash-based geopolymer as a novel photocatalyst for degradation of dye from wastewater. Particuology 11:353–358. https://doi.org/10.1016/J.PARTIC.2012.10.007
104. Setthaya N, Chindaprasirt P, Yin S, Pimraksa K (2017) TiO2-zeolite photocatalysts made of metakaolin and rice husk ash for removal of methylene blue dye. Powder Technol 313:417–426. https://doi.org/10.1016/J.POWTEC.2017.01.014
105. Ökte AN, Karamanis D, Tuncel D (2014) Dual functionality of TiO2-flyash nanocomposites: water vapor adsorption and photocatalysis. Catal Today 230:205–213. https://doi.org/10.1016/J.CATTOD.2014.01.031
106. Visa M, Duta A (2013) Methyl-orange and cadmium simultaneous removal using fly ash and photo-Fenton systems. J Hazard Mater 244–245:773–779. https://doi.org/10.1016/J.JHAZMAT.2012.11.013
107. Kanakaraju D, Bin-Ya MH, Lim YC, Pace A (2020) Combined Adsorption/Photocatalytic dye removal by copper-titania-fly ash composite. Surf Interfaces 19:100534. https://doi.org/10.1016/J.SURFIN.2020.100534
108. El Mragui A, Zegaoui O, Daou I (2019) Esteves da Silva JCG (2019) Preparation, characterization, and photocatalytic activity under UV and visible light of Co, Mn, and Ni mono-doped and (P, Mo) and (P, W) co-doped TiO2 nanoparticles: a comparative study. Environ Sci Pollut Res 2820(28):25130–25145. https://doi.org/10.1007/S11356-019-04754-6
109. Dagar A, Narula AK (2018) Visible-light induced photodegradation of organic contaminants in water using Fe_3O_4 nanoparticles modified polypyrrole/fly ash cenosphere composite. Russ J Phys Chem 92:2853–2860. https://doi.org/10.1134/S0036024419010060
110. Sun YX, Zhang J (2013) Photocatalytic degradation of methyl orange and phenol by BiVO4-loaded fly ash cenospheres (FACs) composite. Adv Mater Res 821–822:471–475. https://doi.org/10.4028/WWW.SCIENTIFIC.NET/AMR.821-822.471
111. Zhao Z, Lei Y, Liu W et al (2017) Fly ash cenospheres as multifunctional supports of g-C3N4/N-TiO2 with enhanced visible-light photocatalytic activity and adsorption. Adv Powder Technol 28:3233–3240. https://doi.org/10.1016/J.APT.2017.09.035
112. Giribabu PVS, Swaminathan G (2015) Synergetic degradation of reactive dye Acid Red 1 by cobalt-doped lignite fly ash. New pub Balaban 57:16955–16962. https://doi.org/10.1080/19443994.2015.1082509
113. Visa M, Andronic L, Duta A (2015) Fly ash-TiO2 nanocomposite material for multi-pollutants wastewater treatment. J Environ Manag 150:336–343. https://doi.org/10.1016/J.JENVMAN.2014.10.026
114. Gilja V, Katancic Z, Krehula LK et al (2019) Eflciency of TiO2 catalyst supported by modified waste fly ash during photodegradation of RR45 dye. IEEE J Sel Top Quantum Electron 26:292–300. https://doi.org/10.1515/SECM-2019-0017/MACHINEREADABLECITATION/RIS
115. Wang G (2011) Photocatalytic degradation of reactive brilliant blue KN-R by N, Fe- TiO2/FFA. Adv Mater Res 183–185:2028–2031. https://doi.org/10.4028/WWW.SCIENTIFIC.NET/AMR.183-185.2028
116. Chen H, Zhao L, Xiang Y et al (2015) A novel Zn–TiO2/C@SiO2 nanoporous material on rice husk for photocatalytic applications under visible light. New Pub Balaban 57:9660–9670. https://doi.org/10.1080/19443994.2015.1035339
117. Huo P, Yan Y, Li S et al (2010) Floating photocatalysts of fly-ash cenospheres supported AgCl/TiO2 films with enhanced Rhodamine B photodecomposition activity. Desalination 256:196–200. https://doi.org/10.1016/J.DESAL.2010.01.012
118. G. Sudha ES, (2015) Synthesis, Characterization and Photocatalytic Study of Cerium Oxide/Zeolite-NaX Catalyst with Brilliant Green Dye Degradation. J Adv Chem Sci 19:117–120
119. Zhang YJ, He PY, Zhang YX, Chen H (2018) A novel electroconductive graphene/fly ash-based geopolymer composite and its photocatalytic performance. Chem Eng J 334:2459–2466. https://doi.org/10.1016/J.CEJ.2017.11.171
120. Zhang YJ, He PY, Yang MY, Kang L (2017) A new graphene bottom ash geopolymeric composite for photocatalytic H2 production and degradation of dyeing wastewater. Int J Hydrogen

Energy 42:20589–20598. https://doi.org/10.1016/J.IJHYDENE.2017.06.156
121. Lu Z, Zhou W, Huo P et al (2013) Performance of a novel TiO2 photocatalyst based on the magnetic floating fly-ash cenospheres for the purpose of treating waste by waste. Chem Eng J 225:34–42. https://doi.org/10.1016/J.CEJ.2013.03.077
122. Lu Z, Huo P, Luo Y et al (2013) Performance of molecularly imprinted photocatalysts based on fly-ash cenospheres for selective photodegradation of single and ternary antibiotics solution. J Mol Catal A Chem 378:91–98. https://doi.org/10.1016/J.MOLCATA.2013.06.001
123. Saravanan R, Gracia F, Stephen A (2017) Basic principles, mechanism, and challenges of photocatalysis. Nanocompos Vis Light Induced Photocatal. https://doi.org/10.1007/978-3-319-62446-4_2
124. Darvishi Cheshmeh Soltani R, Khataee AR, Mashayekhi M (2015) Photocatalytic degradation of a textile dye in aqueous phase over ZnO nanoparticles embedded in biosilica nanobiostructure. New pub Balaban 57:13494–13504. https://doi.org/10.1080/19443994.2015.1058193
125. Subash B, Krishnakumar B, Sreedhar B et al (2013) Highly active WO3–Ag–ZnO photocatalyst driven by day light illumination. Superlattices Microstruct 54:155–171. https://doi.org/10.1016/J.SPMI.2012.11.009
126. Peng X, Luan Z, Ding J et al (2005) Ceria nanoparticles supported on carbon nanotubes for the removal of arsenate from water. Mater Lett 59:399–403. https://doi.org/10.1016/J.MATLET.2004.05.090
127. Ahmed S, Rasul MG, Martens WN et al (2010) Heterogeneous photocatalytic degradation of phenols in wastewater: a review on current status and developments. Desalination 261:3–18. https://doi.org/10.1016/J.DESAL.2010.04.062
128. Ranjan Mishra S, Gadore V, Ahmaruzzaman M (2022) Nanostructured composite materials for treatment of dye contaminated water. Nanohybrid materials for water purification. Springer, Singapore, pp 97–120
129. Gadore V, Mishra SR, Ahmaruzzaman M (2023) One-pot synthesis of CdS/CeO2 heterojunction nanocomposite with tunable bandgap for the enhanced advanced oxidation process. Sci Rep 13:7708. https://doi.org/10.1038/s41598-023-34742-3
130. Mishra SR, Gadore V, Ahmaruzzaman M (2023) Inorganic–organic hybrid quantum dots for AOP-mediated photodegradation of ofloxacin and para-nitrophenol in diverse water matrices. Npj Clean Water. 6:1–24. https://doi.org/10.1038/s41545-023-00291-5
131. Mishra SR, Gadore V, Ahmaruzzaman M (2023) Development of high-performance bi-functional novel CdSnS2 atom cluster for adsorption of Rose Bengal and AOP-assisted degradation of Methylene Blue. Environ Sci Water Res Technol 9:586–602. https://doi.org/10.1039/D2EW00654E
132. Mishra SR, Gadore V, Ghotekar S, Ahmaruzzaman M (2023) Insights into the enhanced photocatalytic and antioxidant properties of novel biogenically synthesised β-In2S3 quantum dots. Int J Environ Anal Chem. https://doi.org/10.1080/03067319.2023.2186228
133. Zhu S, Wang D (2017) Photocatalysis: basic principles, diverse forms of implementations and emerging scientific opportunities. Adv Energy Mater 7:1700841. https://doi.org/10.1002/AENM.201700841
134. Song J, Wang X, Bu Y et al (2017) Photocatalytic enhancement of floating photocatalyst: layer-by-layer hybrid carbonized chitosan and Fe-N- codoped TiO2 on fly ash cenospheres. Appl Surf Sci 391:236–250. https://doi.org/10.1016/J.APSUSC.2016.04.021
135. Neelavannan MG, Ahmed Basha C (2008) Electrochemical-assisted photocatalytic degradation of textile washwater. Sep Purif Technol 61:168–174. https://doi.org/10.1016/J.SEPPUR.2007.10.009
136. Menon SG, Kulkarni SD, Choudhari KS, Santhosh C (2016) Diffusion-controlled growth of CuAl2O4 nanoparticles: effect of sintering and photodegradation of methyl orange. J Exp Nanosci 11:1227–1241. https://doi.org/10.1080/17458080.2016.1209585
137. Mangalam J, Kumar M, Sharma M, Joshi M (2019) High adsorptivity and visible light assisted photocatalytic activity of silver/reduced graphene oxide (Ag/rGO) nanocomposite for wastewater treatment. Nano-Struct Nano-Objects 17:58–66. https://doi.org/10.1016/J.NANOSO.2018.11.003
138. Taourati R, Khaddor M, El Kasmi A (2019) Stable ZnO nanocatalysts with high photocatalytic activity for textile dye treatment. Nano-Struct Nano-Objects 18:100303. https://doi.org/10.1016/J.NANOSO.2019.100303
139. Belviso C (2018) State-of-the-art applications of fly ash from coal and biomass: a focus on zeolite synthesis processes and issues. Prog Energy Combust Sci 65:109–135. https://doi.org/10.1016/J.PECS.2017.10.004
140. Yilmaz N, Davis SM (2016) Polycyclic aromatic hydrocarbon (PAH) formation in a diesel engine fueled with diesel, biodiesel and biodiesel/n-butanol blends. Fuel 181:729–740. https://doi.org/10.1016/J.FUEL.2016.05.059
141. Li G, Wei W, Shao X et al (2018) A comprehensive classification method for VOC emission sources to tackle air pollution based on VOC species reactivity and emission amounts. J Environ Sci 67:78–88. https://doi.org/10.1016/J.JES.2017.08.003
142. Ma X, Li S, Hou Y et al (2022) Adsorption of low-concentration organic pollutants from typical coal-fired power plants by activated carbon injection. Process Saf Environ Prot 159:1174–1183. https://doi.org/10.1016/J.PSEP.2022.02.002
143. Ge JC, Choi NJ (2017) Fabrication of functional polyurethane/rare earth nanocomposite membranes by electrospinning and its VOCs absorption capacity from air. Nanomaterials 7:60. https://doi.org/10.3390/NANO7030060
144. Kim HJ, Yoon JW, Il CK et al (2013) Ultraselective and sensitive detection of xylene and toluene for monitoring indoor air pollution using Cr-doped NiO hierarchical nanostructures. Nanoscale 5:7066–7073. https://doi.org/10.1039/C3NR01281F
145. Rayalu SS, Meshram SU, Biniwale RB et al (2006) Volatile organic carbon monitoring in indoor environment using a versatile hydrophobic flyash-based zeolite as adsorbent. Curr Sci 91:497–503
146. Kim HJ, Pant HR, Choi NJ, Kim CS (2013) Composite electrospun fly ash/polyurethane fibers for absorption of volatile organic compounds from air. Chem Eng J 230:244–250. https://doi.org/10.1016/J.CEJ.2013.06.090
147. Ahmaruzzaman M, Gupta VK (2012) Application of coal fly ash in air quality management. Ind Eng Chem Res 51:15299–15314. https://doi.org/10.1021/IE301336M/ASSET/IMAGES/IE-2012-01336M_M004.GIF
148. Qian Q, Gong C, Zhang Z, Yuan G (2015) Removal of VOCs by activated carbon microspheres derived from polymer: a comparative study. Adsorption 21:333–341. https://doi.org/10.1007/S10450-015-9673-9/FIGURES/8
149. Kim HJ, Pant HR, Choi NJ, Kim CS (2014) Fly ash/polyurethane thin film for the adsorption of volatile organic compounds (VOCs) from air. Fibers Polym 15:1393–1398. https://doi.org/10.1007/S12221-014-1393-3/METRICS
150. Peloso A, Rovatti M, Ferraiolo G (1983) Fly ash as adsorbent material for toluene vapours. Resour Conserv 10:211–220. https://doi.org/10.1016/0166-3097(83)90015-9
151. Rovatti M, Peloso A, Ferraiolo G (1988) Susceptibility to regeneration of fly ash as an adsorbent material. Resour, Conserv Recycl 1(2):137–143. https://doi.org/10.1016/0921-3449(88)90050-X

152. Rovatti M, Bisi M, Ferraiolo G (1992) High added value products from difficult wastes. Resour Conserv Recycl 7:271–283. https://doi.org/10.1016/0921-3449(92)90022-T
153. Rothenberg SJ, Mettzler G, Poliner J et al (1991) Adsorption kinetics of vapor-phase m-xylene on coal fly ash. Environ Sci Technol 25:930–935. https://doi.org/10.1021/ES00017A016/ASSET/ES00017A016.FP.PNG_V03
154. Eiceman GA, Vandiver VJ (1983) Adsorption of polycyclic aromatic hydrocarbons on fly ash from a municipal incinerator and a coal-fired power plant. Atmos Environ 17:461–465. https://doi.org/10.1016/0004-6981(83)90119-1
155. Low GKC, Batley GE (1988) Comparative studies of adsorption of polycyclic aromatic hydrocarbons by fly ashes from the combustion of some australian coal. Environ Sci Technol 22:322–327. https://doi.org/10.1021/ES00168A013/ASSET/ES00168A013.FP.PNG_V03
156. Liu J, Wang T, Shi N et al (2022) Enhancing the interaction between Mn and Ce oxides supported on fly ash with organic acid ligands interface modification for effective VOC removal: a combined experimental and DFT + U study. Fuel 313:123043. https://doi.org/10.1016/J.FUEL.2021.123043
157. Liu J, Shi N, Wang T et al (2021) Significant enhancement of VOCs conversion by facile mechanochemistry coupled MnO2 modified fly ash: Mechanism and application. Fuel 304:121443. https://doi.org/10.1016/J.FUEL.2021.121443
158. Wang W, Zhao Z, Liu F, Wang S (2005) Study of NO/NOx removal from flue gas contained fly ash and water vapor by pulsed corona discharge. J Electrostat 63:155–164. https://doi.org/10.1016/J.ELSTAT.2004.10.002
159. Rokni E, Panahi A, Ren X, Levendis YA (2016) Curtailing the generation of sulfur dioxide and nitrogen oxide emissions by blending and oxy-combustion of coals. Fuel 181:772–784. https://doi.org/10.1016/J.FUEL.2016.05.023
160. Rubio B, Izquierdo MT, Mayoral MC et al (2007) Unburnt carbon from coal fly ashes as a precursor of activated carbon for nitric oxide removal. J Hazard Mater 143:561–566. https://doi.org/10.1016/J.JHAZMAT.2006.09.074
161. Rubel A, Andrews R, Gonzalez R et al (2005) Adsorption of Hg and NOX on coal by-products. Fuel 84:911–916. https://doi.org/10.1016/J.FUEL.2005.01.006
162. Hwang JY (2002) Unburned carbon from fly ash for mercury adsorption: I: separation and characterization of unburned carbon. J Miner Mater Charact Eng 1:39
163. Mercedes Maroto-Valer M, Taulbee DN, Schobert HH et al (1999) Use of unburned carbon in fly ash as precursor for the development of activated carbons. Int ash Util Symp 19:1–18
164. Tokunaga O, Namba H, Suzuki N (1985) Enhancement of removal of SO2 and NOx by powdery materials in radiation treatment of exhaust gases. Int J Appl Radiat Isot 36:807–812. https://doi.org/10.1016/0020-708X(85)90032-8
165. Jayaram S, Castle GSP, Chang JS et al (1996) Semipilot plant pulse energized cold-precharger electrostatic precipitator tests for collection of moderately high resistivity flyash particles. IEEE Trans Ind Appl 32:851–857. https://doi.org/10.1109/28.511641
166. Helfritch DJ (1993) SO2 and NOx removal from flue gas by means of lime spray dryer followed by electron beam irradiation. Non-Thermal Plasma Tech Pollut Control. https://doi.org/10.1007/978-3-642-78476-7_3
167. Tsukamoto S, Namihira T, Wang D et al (2001) Effects of fly ash on NOx removal by pulsed streamers. IEEE Trans Plasma Sci 29:29–36. https://doi.org/10.1109/27.912938
168. Zhao Z (1996) Investigation on the removal of NO and NO~ x from Flue gas using a pulsed corona discharge accounting for flyash and humidity effects. Chin J Environ Sci 17:27–30
169. Yu CJ, Xu F, Luo ZY et al (2009) Influences of water vapor and fly ash addition on NO and SO_2 gas conversion efficiencies enhanced by pulsed corona discharge. J Electrostat 67:829–834. https://doi.org/10.1016/J.ELSTAT.2009.06.003
170. Tsuchiai H, Ishizuka T, Nakamura H et al (1996) Removal of sulfur dioxide from flue gas by the absorbent prepared from coal ash: effects of nitrogen oxide and water vapor. Ind Eng Chem Res 35:851–855. https://doi.org/10.1021/IE950322P/ASSET/IMAGES/MEDIUM/IE950322PE00004.GIF
171. Jozewicz W, Rochelle GT (1986) Fly ash recycle in dry scrubbing. Environ Prog 5:219–224. https://doi.org/10.1002/EP.670050405
172. Brown K, Huang H, Allen J, Livengood C (1988) Combined nitrogen oxides/sulfur dioxide control in a spray-dryer/fabric-filter system. Energy Syst Div. https://doi.org/10.2172/7178213
173. Tsuchiai H, Ishizuka T, Ueno T et al (1995) Highly active absorbent for so2 removal prepared from coal fly ash. Ind Eng Chem Res 34:1404–1411. https://doi.org/10.1021/IE00043A048/ASSET/IE00043A048.FP.PNG_V03
174. Zheng J, Wang J, Yang F et al (2023) Influence and mechanism of the adsorption and reactions of residual NH3, NO, and O2 on coal ash after the selective noncatalytic reduction process. Fuel 343:127826. https://doi.org/10.1016/J.FUEL.2023.127826
175. Wang Y, Ma S, Wang X et al (2022) Study on NO catalytic oxidation by manganese-based catalysts supported on high alumina fly ash. Chin J Process Eng 22:1262. https://doi.org/10.12034/J.ISSN.1009-606X.221416
176. Zhao S, Song K, Zhu J et al (2022) Gd-Mn-Ti composite oxides anchored on waste coal fly ash for the low-temperature catalytic reduction of nitrogen oxide. Sep Purif Technol 302:122119. https://doi.org/10.1016/J.SEPPUR.2022.122119
177. Duan X, Dou J, Zhao Y et al (2020) A study on Mn-Fe catalysts supported on coal fly ash for low-temperature selective catalytic reduction of NOX in Flue gas. Catalyst 10:1399. https://doi.org/10.3390/CATAL10121399
178. Qi K, Xie J, Mei D et al (2018) The utilization of fly ash-MnOx/FA catalysts for NOx removal. Mater Res Express 5:065526. https://doi.org/10.1088/2053-1591/AACD8E
179. Li Y, Gao L, Zhang J et al (2022) Synergetic utilization of microwave - assisted fly ash and carbide slag for simultaneous desulfurization and denitrification: high efficiency, low cost and catalytic mechanism. Chem Eng J 437:135488. https://doi.org/10.1016/J.CEJ.2022.135488
180. Liu M, Zhang L, Zhou W et al (2020) The mechanism of microwave-induced discharge between submillimeter active coke. Plasma Sources Sci Technol 29:75015
181. Matsushima N, Li Y, Nishioka M et al (2004) Novel dry-desulfurization process using Ca(OH) 2/fly ash sorbent in a circulating fluidized bed. Environ Sci Technol 38:6867–6874. https://doi.org/10.1021/ES035373P/ASSET/IMAGES/MEDIUM/ES035373PE00010.GIF
182. Allen D, Hayhurst AN (1996) Reaction between gaseous sulfur dioxide and solid calcium oxide mechanism and kinetics. J Chem Soc Faraday Trans 92:1227–1238. https://doi.org/10.1039/FT9969201227
183. Gupta VK, Mittal A, Gajbe V, Mittal J (2008) Adsorption of basic fuchsin using waste materials—bottom ash and deoiled soya—as adsorbents. J Colloid Interface Sci 319:30–39. https://doi.org/10.1016/J.JCIS.2007.09.091
184. Gupta VK, Carrott PJM, Ribeiro Carrott MML, Suhas, (2009) Low-cost adsorbents: growing approach to wastewater treatment: a review. Crit Rev Environ Sci Technol 39:783–842. https://doi.org/10.1080/10643380801977610
185. Ishizuka T, Tsuchiai H, Murayama T et al (2000) Preparation of active absorbent for dry-type flue gas desulfurization from calcium oxide, coal fly ash, and gypsum. Ind Eng Chem Res 39:1390–1396. https://doi.org/10.1021/IE990699L/ASSET/IMAGES/MEDIUM/IE990699LE00001.GIF

186. Renedo MJ, Fernández J (2002) Preparation, characterization, and calcium utilization of fly Ash/Ca(OH)2 sorbents for dry desulfurization at low temperature. Ind Eng Chem Res 41:2412–2417. https://doi.org/10.1021/IE010938G/ASSET/IMAGES/LARGE/IE010938GF00004.JPEG
187. Al-Shawabkeh A, Maisuda H, Hasatani M (1995) Comparative reactivity of treated FBC- and PCC-Fly ash for SO_2 removal. Can J Chem Eng 73:678–685. https://doi.org/10.1002/CJCE.54507030511
188. Davini P (1996) Investigation of the SO2 adsorption properties of Ca(OH)2-fly ash systems. Fuel 75:713–716. https://doi.org/10.1016/0016-2361(95)00303-7
189. Li Y, Nishioka M, Sadakata M (1999) High calcium utilization and gypsum formation for dry desulfurization process. Energy Fuels 13:1015–1020. https://doi.org/10.1021/EF9802781/ASSET/IMAGES/LARGE/EF9802781F00006.JPEG
190. Davini P (1995) Investigation of flue gas desulphurization by fly ash and calcium hydroxide mixtures. Resour Conserv Recycl 15:193–201. https://doi.org/10.1016/0921-3449(95)00029-1
191. Davini P (2002) Flue gas treatment by activated carbon obtained from oil-fired fly ash. Carbon N Y 40:1973–1979. https://doi.org/10.1016/S0008-6223(02)00049-0
192. Guo Q, Chen M, Zhang J et al (2022) Microwave-assisted industrial wastes of fly ash and carbide slag as adsorbents for simultaneous desulfurization and denitrification. Sep Purif Technol 303:122176. https://doi.org/10.1016/J.SEPPUR.2022.122176
193. Wang KQ, Gao XM, Lin B et al (2023) An efficient calcium-based sorbent for flue gas dry-desulfurization: promotion roles of nitrogen oxide and oxygen. RSC Adv 13:1312–1319. https://doi.org/10.1039/D2RA05769G
194. Qi L, Luo J, Wang W, Zhao W (2023) Adsorption of SO2 from sintering flue gas by alkali modified fly ash in electrostatic precipitator. Sep Sci Technol 58:1237–1251. https://doi.org/10.1080/01496395.2023.2180392
195. Tsuchiai H, Ishizuka T, Nakamura H et al (1996) Study of flue gas desulfurization absorbent prepared from coal fly ash: effects of the composition of the absorbent on the activity. Ind Eng Chem Res 35:2322–2326. https://doi.org/10.1021/IE9507033/ASSET/IMAGES/LARGE/IE9507033F00005.JPEG
196. Lee KT, Mohamed AR, Bhatia S, Chu KH (2005) Removal of sulfur dioxide by fly ash/CaO/CaSO4 sorbents. Chem Eng J 114:171–177. https://doi.org/10.1016/J.CEJ.2005.08.020
197. Lee KT, Bhatia S, Mohamed AR (2005) Preparation and characterization of sorbents prepared from ash (waste material) for sulfur dioxide (SO2) removal. J Mater Cycles Waste Manag 7:16–23. https://doi.org/10.1007/S10163-004-0121-2/METRICS
198. Zhou F, Cheng J, Liu J et al (2018) Improving physicochemical properties of upgraded Indonesian lignite through microwave irradiation with char adsorbent. Fuel 218:275–281. https://doi.org/10.1016/J.FUEL.2018.01.044
199. Wang Z, Liu J, Yang Y et al (2020) Regenerable CoxMn3−xO4 spinel sorbents for elemental mercury removal from syngas: experimental and DFT studies. Fuel 266:117105. https://doi.org/10.1016/J.FUEL.2020.117105
200. Song G, Deng R, Yao Z et al (2020) Anthracite coal-based activated carbon for elemental Hg adsorption in simulated flue gas: preparation and evaluation. Fuel 275:117921. https://doi.org/10.1016/J.FUEL.2020.117921
201. Liu Z, Liu D, Zhao B et al (2020) Mercury removal based on adsorption and oxidation by fly ash: a review. Energy Fuels 34:11840–11866. https://doi.org/10.1021/ACS.ENERGYFUELS.0C02209/ASSET/IMAGES/LARGE/EF0C02209_0013.JPEG
202. Yang J, Zhao Y, Zhang S et al (2017) Mercury removal from flue gas by magnetospheres present in fly ash: role of iron species and modification by HF. Fuel Process Technol 167:263–270. https://doi.org/10.1016/J.FUPROC.2017.07.016
203. Wang F, Wang S, Meng Y et al (2016) Mechanisms and roles of fly ash compositions on the adsorption and oxidation of mercury in flue gas from coal combustion. Fuel 163:232–239. https://doi.org/10.1016/J.FUEL.2015.09.065
204. Świerczok A, Jędrusik M, Łuszkiewicz D (2020) Reduction of mercury emissions from combustion processes using electrostatic precipitators. J Electrostat 104:103421. https://doi.org/10.1016/J.ELSTAT.2020.103421
205. Xing L, Xu Y, Zhong Q (2012) Mn and Fe modified fly ash as a superior catalyst for elemental mercury capture under air conditions. Energy Fuels 26:4903–4909. https://doi.org/10.1021/EF3005256/ASSET/IMAGES/EF-2012-005256_M006.GIF
206. Xu Y, Zhong Q, Xing L (2014) Gas-phase elemental mercury removal from flue gas by cobalt-modified fly ash at low temperatures. Environ Technol 35:2870–2877. https://doi.org/10.1080/09593330.2014.924569
207. Zhang Y, Duan W, Liu Z, Cao Y (2014) Effects of modified fly ash on mercury adsorption ability in an entrained-flow reactor. Fuel 128:274–280. https://doi.org/10.1016/J.FUEL.2014.03.009
208. Zhang Y, Zhao L, Guo R et al (2015) Mercury adsorption characteristics of HBr-modified fly ash in an entrained-flow reactor. J Environ Sci 33:156–162. https://doi.org/10.1016/J.JES.2015.01.011
209. Song N, Teng Y, Wang J et al (2014) Effect of modified fly ash with hydrogen bromide on the adsorption efficiency of elemental mercury. J Therm Anal Calorim 116:1189–1195. https://doi.org/10.1007/S10973-014-3701-Y/FIGURES/7
210. Yang J, Zhao Y, Zhang J, Zheng C (2016) Removal of elemental mercury from flue gas by recyclable CuCl2 modified magnetospheres catalyst from fly ash: part 1 catalyst characterization and performance evaluation. Fuel 164:419–428. https://doi.org/10.1016/J.FUEL.2015.08.012
211. Xu W, Wang H, Zhu T et al (2013) Mercury removal from coal combustion flue gas by modified fly ash. J Environ Sci 25:393–398. https://doi.org/10.1016/S1001-0742(12)60065-5
212. Zhang Y, Zhao L, Guo R et al (2017) Influences of NO on mercury adsorption characteristics for HBr modified fly ash. Int J Coal Geol 170:77–83. https://doi.org/10.1016/J.COAL.2016.10.002
213. Wang S, Zhang Y, Gu Y et al (2019) Coupling of bromide and on-line mechanical modified fly ash for mercury removal at a 1000 MW coal-fired power plant. Fuel 247:179–186. https://doi.org/10.1016/J.FUEL.2019.03.053
214. Li L, Pan SW, Hu JJ et al (2013) Experimental research on fly ash modified adsorption of mercury removal efficiency of flue gas. Adv Mater Res 800:132–138. https://doi.org/10.4028/WWW.SCIENTIFIC.NET/AMR.800.132
215. He P, Zhang X, Peng X et al (2015) Enhancement using external magnetic field on mercury capture by fly ash. Fuel 162:211–214. https://doi.org/10.1016/J.FUEL.2015.09.014
216. Yang S, Yan N, Guo Y et al (2011) Gaseous elemental mercury capture from flue gas using magnetic nanosized (Fe3-xMnx)1-δO4. Environ Sci Technol 45:1540–1546. https://doi.org/10.1021/ES103391W/SUPPL_FILE/ES103391W_SI_001.PDF
217. Zeng X, Xu Y, Zhang B et al (2017) Elemental mercury adsorption and regeneration performance of sorbents FeMnOx enhanced via non-thermal plasma. Chem Eng J 309:503–512. https://doi.org/10.1016/J.CEJ.2016.10.047
218. Shi M, Luo G, Zhu H et al (2019) Surface modification of fly ash by non-thermal air plasma for elemental mercury removal from coal-fired flue gas. Environ Technol 42:306–317. https://doi.org/10.1080/09593330.2019.1627423

219. Wang J, Jiang C, Shi L et al (2022) Hg0 Removal by a palygorskite and fly ash supported MnO_2-CeO_2 catalyst at low temperature. Catalyst 12:662. https://doi.org/10.3390/CATAL12060662
220. Qi L, Wang X, Wang W et al (2022) Mercury removal from coal combustion flue gas by pyrite-modified fly ash adsorbent. Environ Sci Pollut Res 29:39228–39238. https://doi.org/10.1007/S11356-022-18963-Z/FIGURES/11
221. Xin F, Xiao R, Zhao Y, Zhang J (2022) Surface sulfidation modification of magnetospheres from fly ash for elemental mercury removal from coal combustion flue gas. Chem Eng J 436:135212. https://doi.org/10.1016/J.CEJ.2022.135212
222. Wang J, Li D, Ju F et al (2015) Supercritical hydrothermal synthesis of zeolites from coal fly ash for mercury removal from coal derived gas. Fuel Process Technol 136:96–105. https://doi.org/10.1016/J.FUPROC.2014.10.020
223. Ma L, Han L, Chen S et al (2019) Rapid synthesis of magnetic zeolite materials from fly ash and iron-containing wastes using supercritical water for elemental mercury removal from flue gas. Fuel Process Technol 189:39–48. https://doi.org/10.1016/J.FUPROC.2019.02.021
224. Kunecki P, Wdowin M, Hanc E (2023) Fly ash-derived zeolites and their sorption abilities in relation to elemental mercury in a simulated gas stream. J Clean Prod 391:136181. https://doi.org/10.1016/J.JCLEPRO.2023.136181
225. Zhu T, Kuang J, Xu W et al (2012) Study on mercury adsorption performance of modified fly ash. Adv Mater Res 343–344:246–249. https://doi.org/10.4028/WWW.SCIENTIFIC.NET/AMR.343-344.246
226. López-Antón MA, Abad-Valle P, Díaz-Somoano M et al (2009) The influence of carbon particle type in fly ashes on mercury adsorption. Fuel 88:1194–1200. https://doi.org/10.1016/J.FUEL.2007.07.029